Journal of Superconductivity and Novel Magnetism (2019) 32:127–144
https://doi.org/10.1007/s10948-018-4929-8

REVIEW PAPER

Superparamagnetic Properties and Significant Applications of Iron Oxide Nanoparticles for Astonishing Efficacy—a Review

S. Mangala Devi[1] · A. Nivetha[1] · I. Prabha[1]

Received: 26 July 2018 / Accepted: 28 October 2018 / Published online: 3 November 2018

Abstract

This paper reviewed the comprehensive literature survey on the physical, chemical, and the catalytic properties and applications of iron oxide nanoparticles. In recent years, iron oxide has made a versatile progress due to its outstanding magnetic property. The average crystallite size was reported in previous literatures in the range of 10–45 nm using Scherrer's formula. The powder morphology was found to deliberate quasi-spherical and predominantly spherical shape. The specific surface area as measured by N_2 adsorption BET isotherm was reported in the range of 17.6–26.21 m^2/g. Depending on the synthesis pathway there was, an inverse or normal spinel structure could be achieved. X-ray diffraction analysis revealed the crystallite size in the range between 8 and 42 nm. Fourier transform infrared spectroscopy reported the changes in functional group, stretching vibrations in the iron oxide nanoparticles. Scanning electron microscopy analysis showed most of Fe_3O_4 nanoparticles were in spherical morphology with the particle size range between 10 and 26 nm. Vibrating sample magnetometer reported the magnetization value for Fe_3O_4 nanoparticles.

Keywords Magnetite · Spinel · Superparamagnetism · Vibration sample magnetometer · Applications · Reusability

1 Introduction

Iron was originated as the most common element on Earth's outer and inner core which was found as one fourth of the elements in the Earth's crust. Iron was the single and most important metal in human civilization and was refined and used on the scale of more than a billion tones of year, and more than 90% of refined metal was iron. Iron ore was widely distributed and reduced in a blast furnace with the support of coke and limestone. It was the most abundant transition metal and showed enormous applications in all fields. Iron has been formed with its number of oxides, and among them, Fe_3O_4 was a naturally occurring mineral magnetite which consisted of many impurities magnetized by lightning the strike. The permanent magnet has been known to ancient man as lodestones and used in navigational compasses for at least 800 years [1]. During the past few decades, the most active research areas in advanced materials have led to the synthesis of functional magnetic nanoparticles (MNPs) in nanoscience and nanotechnology [2, 3]. MNPs have revealed distinctive magnetic properties, and other specific properties such as electronic and optical showed a wide range of applications [4]. In recent studies, the interacting magnetic nanoparticles have revealed a very wide area in synthesis, characterization, and applications of novel composites [5, 6]. Size of the nanoparticles was the important parameter to determine the different properties of the material. The properties of nanosized materials were different from that of the corresponding bulk materials, which have been reported [7, 8]. Compared to atomic or bulky materials, nanosized materials have showed better physical and chemical properties due to their mesoscopic effect, small object effect, quantum size effect, surface effect, etc. Iron oxides were found to be familiar compounds and common in nature and could be readily synthesized in the laboratory conditions.

Eight supplementary iron oxides have been identified [9] as derivatives of iron, and mainly ferrous and ferric iron oxides existed in seven crystalline phases, such as α-Fe_2O_3 (hematite), γ-Fe_2O_3 (maghemite), Fe_3O_4 (magnetite), and $Fe_{1-x}O$ (wustite), and β and ε-Fe_2O_3 phases were found as the less

✉ I. Prabha
iprabha2007@gmail.com

S. Mangala Devi
sdevi3011@gmail.com

[1] Department of Chemistry, Bharathiar University, 641 046, Coimbatore, India

commonly found and the low temperature rhombohedral structure of magnetite. Among these iron oxides, in addition to that, hematite (α-Fe_2O_3), maghemite (γ-Fe_2O_3), and magnetite (Fe_3O_4) were very promising and popular candidates due to their polymorphism involving the temperature-induced phase transition. Hematite was one of the most stable iron oxides and n-type semiconductor under ambient conditions. Due to this unique property, it was widely used as catalysts in various chemical reactions, pigments and gas sensors for its low cost and high resistance to corrosion, etc. For the synthesis of magnetite (Fe_3O_4) and maghemite (γ-Fe_2O_3), hematite was used as a starting material, which has been intensively pursued for the fundamental scientific interests and technological applications in the last few decades of iron period. Hematite was an n-type semiconductor with a band gap of 2.3 eV, where the conduction band (CB) has consisted of empty d-orbitals of Fe^{3+} ions and the valence band (VB) was composed of occupied 3d crystal field orbitals of Fe^{3+} with admixture from the oxygen, 2p non-bonding orbitals. Fe^{3+} ions have occupied two thirds of the octahedral sites restricted the ideal hexagonal close-packed O lattice [10, 11]. The structure of γ-Fe_2O_3 is found to be cubic, and each unit of maghemite contains 32 O^{2-} ions as magnetite, $211^1/_3$ are occupied by Fe^{3+} ions and $2^1/_3$ were vacancies. Oxygen anions have been arranged to give a cubic closed packing. The ferric ions were distributed in the tetrahedral sites (eight Fe ions per unit cell) and octahedral sites (the remaining Fe ions and vacancies). So the maghemite was considered as a fully oxidized magnetite and n-type semiconductor with a band gap of 2.0 eV.

Magnetic iron oxides have served humans for centuries. The function of iron oxide nanoparticles as different agents for in vitro diagnostics has been practiced for around half a century [12, 13]. In recent times, Fe_3O_4 was seriously investigated because of their superparamagnetism, high coercivity, and low Curie temperature [14, 15]. Fe_3O_4 has a cubic inverse spinel structure and has Fd3m space group for Fe_3O_4. Magnetite was a black ferrimagnetic mineral containing both Fe^{2+} and Fe^{3+} ions. In Fe_3O_4, oxygen atom has formed a cubic structure, 1/3 of the intersites were tetrahedrally occupied and 2/3 was occupied in octahedral site. The unit cell of Fe_3O_4 has 32 O^{2-} ions which were arranged in regular cubic close packing with the [100] direction. The lattice constant was found to be $a = 0.839$. The crystal structure of Fe_3O_4 consisted of two different iron sites: tetrahedral sites were occupied by Fe (III) and octahedral sites were occupied by both Fe (II) and Fe (III). In general, Fe_3O_4 crystals were distributed with octahedral and mixed octahedral/tetrahedral layer along in the (111) direction [16, 17]. Magnetic iron oxide nanoparticles consisted of two major parts: conserved the magnetic property of magnetic iron oxides and preserved some other properties of iron oxides with the properties of organic molecules. These three iron oxides have unique biochemical, magnetic, catalytic, and biomedical applications. Particularly, bioapplications-based magnetic nanoparticles (NPs) have received much attention due to their unique advantages over other materials. Magnetic nanoparticles were cost-effective to generate magnetite nanoparticles which showed the physical and chemical stability, biocompatibility, and environmental safety [18].

There was a higher surface energy for high-index planes. For the face-centered-cubic, the sequence was arranged to be $\gamma(111) < \gamma(100) < \gamma(110) < \gamma(220)$ and generated the distance between the planes and the central Wulff's point. For this reason, the Fe_3O_4 nanoparticles were surrounded mostly by {111}, and it has been revealed octahedral morphology. The ratio (R) of growth rate was determined by the crystal shape in the <100> direction to <111> direction. In <100> direction, faster growth has led to octahedral particles, while faster growth along the <111> direction could generate cubic particles. To get a variety of morphologies, it is necessary to control the growth rate of different surfaces of the nuclei, and hence, surfactant, templates, or other specific conditions are applied [12, 19, 20]. For the synthesize of monodispersed spherical Fe_3O_4 nanoparticles, both oleic acid and oleylamine were used as surfactants. Xie and co-workers have prepared Fe_3O_4 nanoparticles by utilizing the trichloro-s-triazine (TsT) and a linker molecule. Other routes such as solvothermal methods were also used to synthesize spherical Fe_3O_4 nanoparticles [21, 22].

In this method, right quantities of potassium ferrocene, sodium borohydride, sodium hydroxide, polyvinylpyrrolidone, and alcohol were mixed and heated to 180 °C in an autoclave by this typical process and have been found that the growth of the (111) surface was slow down because of the absorption of hydroxyl group on the (111) facet. There was a change in the shape of the Fe_3O_4 from spherical particles to octahedral particles due to increase in the surfactant concentration [23]. Yang and co-workers have synthesized the monodispersed Fe_3O_4 nanocubes which has a controllable particle sizes of 6–30 nm. Fe $(acac)_3$ was used as a precursor, benzyl ether as a solvent, and 1,2-hexadecanediol, oleic acid (OA), and oleylamine (OAm) as the surfactants. The carboxylic group presented in the oleic acid was bound selectively to crystal surface to control size of nanoparticles. The OAm has been possessed moderately weak, and exhibited isotropic binding to the surface affected the morphology of the Fe_3O_4 nanoparticles. By changing the stabilizers for the fabrication of Fe_3O_4 nanoparticles, they found the use of sodium oleate led to nanocubes. Potassium oleate has been generated a mixture of nanocubes with magnetite nanoparticles of different morphologies [24]. Iron oxide nanomaterial was synthesized by different methods as microwave-assisted synthesis, ultrasonication, co-precipitation, chemical reduction, hydrothermal method, bio-mediated synthesis [25–28], etc.

In Fe_3O_4 nanoparticles, there is a possibility of presence of impurity phases, like α-Fe_2O_3 in the synthesized iron nanoparticles. Liang et al. used the hydrothermal method to synthesize Fe_3O_4 nanoparticles and revealed the reaction time was increased, α-Fe_2O_3 impurities have been decreased, and simultaneously, Fe_3O_4 phase has been increased slowly. Alcala et al. prepared Fe_3O_4 nanoparticles by the mechanical alloying of iron and hematite. The result showed that continuous milling time was extended more than 3 h and there was the formation of pure phase of Fe_3O_4. Hu et al. studied the heat treatment effects on Fe_3O_4 nanoparticles at higher temperature of 650 °C showed that the synthesized particle size was reported to be 48 nm [29, 30].

Iron and iron-based nanoparticles have attracted considerable interest in different areas of research when compared to bulk materials. It showed exclusive properties such as catalytic, magnetic, antioxidant, anti-microbial, and optical property and attained several developments in the field of science, engineering, and technology. Expensive instruments, high energy, toxic reducing agents, maintaining the cell culture, recovery steps, etc. were found to be the list of disadvantages identified in physical-, chemical-, and microbe-mediated syntheses [31, 32]. The critical value of each particle becomes a single domain with a large spin, when the size of nanoparticles becomes smaller, it is called super spin [33]. There were two types of super spins such as superparamagnetism (SPM) which was non-interacting or weakly interacting super spins and strongly interacting spins led to super spin-glass (SSG) [34]. Figure 1 shows the phase diagram of stable iron oxide.

Iron oxide magnetic nanoparticles (Fe_3O_4-MNPs) have the approximate size of 20–30 nm and contained a single magnetic field with a single magnetic moment which exhibited superparamagnetism [3]. When Fe_3O_4 nanoparticles (MNPs) were magnetized in the presence of an external magnet, it was used to study the large surface area to volume ratios, easy functionalization, superparamagnetic property, and also used for various biological applications such as drug delivery,

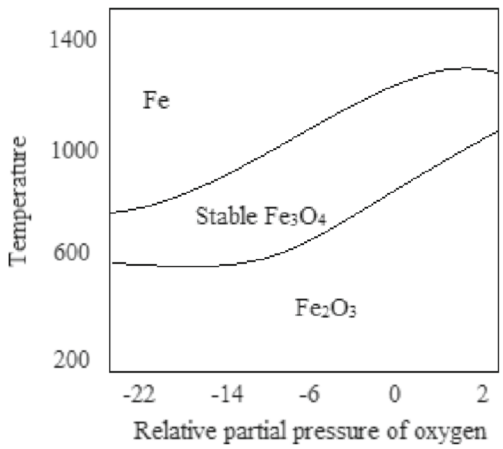

Fig. 1 Phase diagram of stable iron oxide

magnetic resonance imaging (MRI), bio-separation, biomolecular sensors, and magneto-thermal therapy, etc. [35]. It has cubic inverse spinel structure and there has a formation of FCC closed packing by oxygen atoms with interstitial tetrahedral sites and octahedral sites occupied by Fe cations. In the octahedral sites, the electrons jump between Fe^{2+} and Fe^{3+} ions at room temperature [36]. The particles attracted to an external magnetic field, but there was no magnetization when the magnetic field was removed and this was called as superparamagnetism. Using an external magnet, the suspended magnetite nanoparticles were removed without agglomeration [37].

The theory of ferrimagnetism was illustrated by Neel using Fe_3O_4 as an example. Before Neel's work, Fe_3O_4 was classified as a ferromagnet, and magnetization of 4 μB per formula unit has been measured. Neel reported that the tetrahedral and octahedral sub-lattices were anti ferromagnetically aligned in Fe_3O_4 and the Fe^{3+} cations, and each sub-lattice has canceled each other. Hence, the magnetic moment aroused wholly from the moment of the remaining Fe^{2+} cation [38]. The electronic structure of Fe_3O_4 was studied experimentally using photoemission process. It was important to highlight the use of Fe^{2+} and Fe^{3+} ions and the presence of different cations in Fe_3O_4. The true point of charge disproportionation between the different cations was undoubtedly much smaller, and there aroused a question whether it existed at all. Recent work has showed the value below T_V, the charge disproportionation should be "frozen in," and the oxidation states of Fe cations have varied between 2.4+ and 2.9+. In the room temperature, all the Fe_{oct} cations were crystallographically equivalent and Mossbauer spectroscopy explained that all Fe_{oct} were equivalent, even though this was probably a time average [39, 40]. Magnetite has inverse cubic spinel structure according to $[Fe^{3+}]_{Td}[Fe^{2+}\ Fe^{3+}]_{Oh}O_4$ with a half metallic structure and exhibited semiconductive properties because of fast jumping of electrons between Fe^{2+} and Fe^{3+} in the octahedral sublattice evidenced by Mossbauer spectroscopy.

The optical absorption of the iron nanoparticles was studied in the wavelength of 190–900 nm. From the view of scattering theory, the shape of the spectra and wavelength of the maximum optical extinction depend only on the dielectric function of the nanoparticles. For spherical particles, a single peak of destruction spectra appeared and the absorption spectra of colloidal iron nanoparticles were determined. The observation suggested that the stability of colloidal solution and size distribution of nanoparticles depend on the nature of liquid. Due to the interaction of liquid molecules and charged nanoparticles in liquid medium, electrical double layers have been formed around the surface of the generated nanoparticles [41]. Furthermore, acetone has high dipole moment that led to the occurring of adequate electrostatic repulsive force because of the overlapping of strong electrical double layer due to the presence of nanoparticles in colloidal solution of acetone

which was stable without aggregation and precipitation. And, water agglomeration occurred after 2 h due to oxidation and compared with acetone, water decreased in polarity [42]. Figure 2 shows the purification process of magnetite ore by various steps.

Magnetite nanoparticles were synthesized by two-stage continuous flow stirred reactors by aqueous co-precipitation of Fe (II) and Fe (III) salts under alkaline conditions and by heating at 70 °C [43, 44]. Iron salt solution of 0.05 mol Fe/L was continuously pumped in the first stage of the reactor (5 L/h for Fe(II) and 10 L/h for Fe(III)), when there was the addition of NaOH, the pH was adjusted to 12.0. As a result, there was a formation of black precipitate indicating the formation of magnetite. The obtained slurry was kept for 1 h and was washed in cycles of magnetic separation/re-dispersion in distilled water. Finally, the sludge was dried at 40 °C to get powder samples of Fe_3O_4 magnetic nanoparticles [45]. Fe_3O_4 nanoparticles have attracted much interest due to their potential applications in different areas, such as super capacitor electrode materials, adsorption of heavy metal processes, recyclable catalysts for catalytic oxidation of alcohols, magnetic carriers for protein separation, and wastewater treatment [46, 47].

2 Characterization

Iron oxide (Fe_3O_4) nanoparticles were characterized by XRD, BET surface area, SEM, TEM-EDS, TGA/DTA, and VSM analyses. The specific surface area of Fe_3O_4 nanoparticles was characterized by BET analysis. XRD was used to reveal the crystalline nature and crystallite size of Fe_3O_4 nanoparticles using Scherrer's formula. EDS was used for the identification of the elements present in the Fe_3O_4 nanoparticles. SEM and TEM were used to characterize the surface morphology and particle size distribution of the iron nanoparticles. VSM was the technique used to determine the magnetization of the Fe_3O_4 nanoparticles. TGA/DTA analysis was used to confirm the thermal stability of the prepared Fe_3O_4 nanoparticles. Figure 3 shows the flow chart of properties and characterization of Fe_3O_4 nanoparticles.

2.1 BET Analysis of Fe_3O_4 Nanoparticles

BET analysis was used to determine the surface area and pore size distribution at liquid nitrogen temperature. In surface area analysis, nitrogen was used because of its availability in high purity and its strong interaction with most of the solids. Because of the interaction between gaseous and solid phases, it was usually weak and the surface was cooled using liquid N_2 to obtain detectable amounts of adsorption. Cheera et al. synthesized the Fe_3O_4 nanoparticles by ecofriendly method using extract of Pistum sativum. The prepared Fe_3O_4 nanoparticles were characterized by BET surface area analysis. BET was used to study the porous nature and surface area of the PS-Fe_3O_4 magnetic nanoparticle materials. There were loops present in between 0.45 and 0.99 confirmed the sample

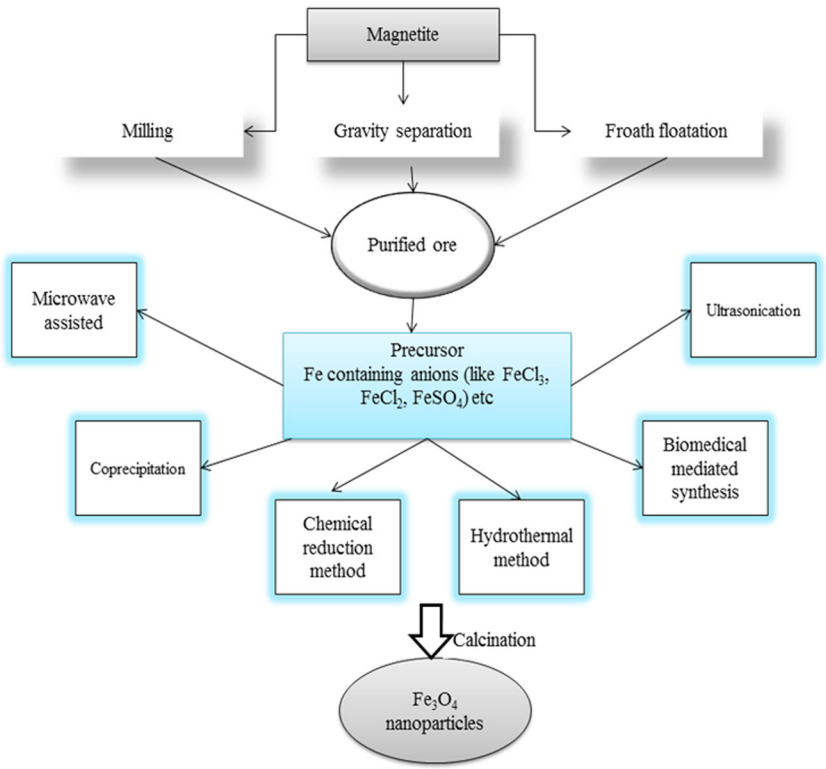

Fig. 2 Purification of magnetite ore

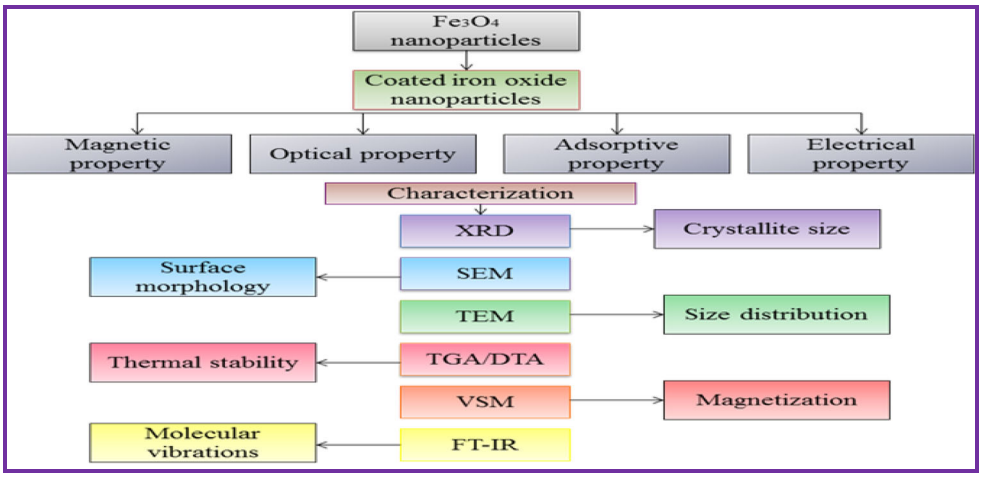

Fig. 3 Flow chart of properties and characterization of Fe_3O_4 nanoparticles

has mesopores on it. The calculated surface area of the nanomaterial was found to be ~ 17.6 $m^2\ g^{-1}$ which was higher than other Fe nanomaterials [48]. Prasad et al. prepared the Fe_3O_4 nanoparticles by green synthesis using Ridge gourd as a starting material. The synthesized RG-Fe_3O_4 nanoparticles were characterized by BET surface area analysis. The porous nature of iron nanoparticles was studied by N_2 adsorption-desorption method, and the surface area was found to be 26.21 $m^2\ g^{-1}$. By Barrett, Joyner, and Halenda (BJH) method, the total pore volume and pore size distribution of Fe_3O_4 nanoparticles were identified to be about 0.134 cm^3/g, and it was a mesoporous material with pore size ranged from 7 to 25 nm [49].

2.2 XRD Analysis of Fe_3O_4 Nanoparticles

X-ray diffraction is a very important experimental technique that has long been used to address all the information and issues related to the crystal structures of solids, including lattice constants, geometry, identification of unknown materials, orientation of single crystal, defects, stresses, average grain size, and strain defects of the Fe_3O_4 nanoparticles. In XRD, a collimated beam of X-rays was made incident on a specimen such as Fe_3O_4 nanoparticles and was diffracted by the crystalline phases according to Bragg's law. Ting et al. synthesized the series of Fe_3O_4 nanoparticles by microemulsion method, and the prepared Fe_3O_4 was characterized by using XRD analysis. Fe_3O_4 consisted of cubic spinel type with single phase, and α-Fe_2O_3 and γ-Fe_2O_3 phases were not observed. And, it was compared with the standard pattern of Fe_3O_4 and resulted the decrement of particle size. The lattice constant of Fe_3O_4 nanoparticles was calculated, and the results showed that Fe_3O_4 nanoparticles were consistent with standard inverse spinel type Fe_3O_4 [50].

Yang et al. synthesized the superparamagnetic iron nanoparticles by co-precipitation method. The synthesized Fe_3O_4 nanoparticles diffraction pattern was nearly close to the crystalline of magnetite. The diffraction peaks were indexed to (2 2 0), (3 1 1), (4 0 0), (4 2 2), (5 1 1), and (4 4 0) planes, and the observed details have been matched with the inverse cubic spinel structure of Fe_3O_4 nanoparticles [51]. Yan et al. prepared the Fe_3O_4 nanoparticles from interior stem wall and epidermal surface of soya bean sprout. The diffraction peaks were indexed to (2 2 0), (3 1 1), (4 0 0), (5 1 1), (4 4 0), and (5 3 3) planes. Both the materials could be indexed with the inverse cubic spinel structure of Fe_3O_4 [52].

Aslibeiki et al. synthesized Fe_3O_4 nanoparticles by thermal decomposition method and calcinated in N_2 atmosphere at 300° (N300) and 350° (N350) as well as air (A300 and A350). XRD pattern reported that both the samples were pure single cubic spinel. The sample of N350 that got the sharp peaks showed that calcination temperature was increased and particle size was also increased. The average particle sizes for the Fe_3O_4 nanoparticles were confirmed to be 8 nm and 12 nm [53]. Superparamagnetic poly (o-Toluidine) (POT)/Fe_3O_4 nanoparticles composite revealed the diffraction peaks indexed to (111), (220), (311) (222), (400), (422), (511), and (440) planes. It was exhibited a spinel (face-centered cubic) Fe_3O_4 and represented the presence of Fe_3O_4 nanoparticles in a prepared material [54]. Silva et al. prepared the fucan-coated and fucan-uncoated magnetites by co-precipitation method, and XRD results revealed that Fe_3O_4 consisted of inverse cubic spinel structure corresponded to (2 2 0), (3 1 1), (4 0 0), (4 2 2), (5 1 1), and (4 4 0) planes and the particle size was identified to be 10 nm using Scherrer's formula. The observed peaks in the same range showed that the coating did not affect the core magnetite. And the fucan-coated in the peak height was decreased and the background becomes noisy due to its amorphous nature [55].

The magnetic Fe_3O_4, Fe_3O_4@SiO_2, and Fe_3O_4@SiO_2@Chol nanoparticles were synthesized by Zhihong Yan et al., and the XRD analysis showed that nanoparticles were in well accordance with one another and it was indicated that cholesterol coating did not damaged the

structure of Fe_3O_4 nanoparticles [56]. Shete et al. synthesized the CS-OA-Fe_3O_4 nanoparticles by alkaline precipitation method, and the XRD results matched very well with standard iron oxide nanoparticles. The main diffraction peaks were obtained with the (hkl) values of (220), (311), (400), (422), and (511) and showed the inverse spinel structure of Fe_3O_4 nanoparticles with the crystallite sizes of 20 nm and 10 nm for bare and OA-CS-coated magnetic nanoparticles respectively. The particle size was decreased when capping with CS-OA, and it was confirmed by peak broadening decreased in intensity after capping [57]. Emre Cevik et al. synthesized the Fe_3O_4-Si (GMA-co-Vfc) nanoparticles, and the material was characterized by XRD analysis. He observed the (111), (220), (311), (400), (422), (511), (440), (620), and (533) peaks resembled the core Fe_3O_4. The broadening of peaks was indicated by small crystal size, and the crystal size was found to be about 9 ± 2 nm [58]. Ali Ebrahimi Fard et al. synthesized the Triethylene-glycol modified Fe_3O_4 nanoparticles by thermal decomposition method. XRD data showed that the Miller indices were found to be (2 2 0), (3 1 1), (2 2 2), (4 0 0), (4 2 2), (5 1 1), (4 4 0), and (5 3 3). These patterns resulted the prepared Fe_3O_4 nanoparticles have cubic spinel structure, and it did not consisted of nil impurities with extremely high crystalline particles. These results were in good unity with the diffraction patterns of bulk magnetite material [59]. Table 1 shows the iron oxide nanoparticles and their physical properties.

Ming et al. prepared the magnetic Fe_3O_4 nanoparticles and it found near to the core magnetite with face-centered cubic structure characterized by XRD [68]. Rahmatollah et al. observed the XRD pattern of magnetite bromochromate and concluded that six diffraction peaks of about (220), (311), (400), (422), (511), and (440) were in accordance with the standard magnetite nanoparticles. The intense and sharp peak revealed that the magnetite nanoparticles were crystalline in nature and the average size of reflection plane (311) was about 42 nm [69].

2.3 EDS Analysis of Fe_3O_4 Nanoparticles

Energy-dispersive spectrometer (EDSs) employed the pulse height analysis which was giving output pulses proportional in height to the X-ray photon energy used in conjunction with a pulse height analyzer (in this case a multichannel type). A solid state detector was used in these spectrometers because of its better energy resolution. Incident X-ray photons caused ionization in the detector and produced an electrical charge amplified by a sensitive preamplifier located close to the detector. Both the detector and pre-amplifier were cooled with liquid nitrogen to minimize the electronic noise. EDS analysis

Table. 1 Physical properties of iron oxide nanoparticles

S .no	Synthesized material	Average diameter	Mean particle size	Morphology	Plane	Phase
1.	EDTA capped magnetite nanoparticles	15 nm	10 nm	Spherical	Plane matches with bare magnetite	Cubic spinel [60]
2.	Iron oxide nanoparticles	200 nm	12 nm	Spherical	(220), (311), (222), (400), (422), (511), (440)	Cubic spinel [61]
3.	Fe_3O_4	Not mentioned	26 nm	Predominantly spherical with hexagonal shaped	Plane matches with bare magnetite [62]	Not mentioned
4.	Fe_3O_4 MNPs and β-cyclodextrin MNPs	8.1 nm and 12 nm	10 and 16	Not mentioned	(220), (311), (400), (422), (511), and (440)	Cubic spinel [63]
5.	Polyacrylic acid coated Fe_3O_4	60 nm	Not mentioned	Spherical	(222), (311), and (440),	Inverse spinel structure [64]
6.	Fe_3O_4-Si(GMA-co-Vfc)	9 ± 2 nm	11.6 ± 0.4 nm	Spherical	(111), (220), (311), (400), (422),(511), (440), (620), and (533) [58, 76]	Not mentioned
7.	Fucan-coated magnetite (Fe_3O_4) nanoparticles	Not mentioned	10 nm	Quasi-spherical	(220), (311), (400), (422), (511), and (440) [55]	Not mentioned
8.	Surfactant-stabilized Fe_3O_4 magnetic nanocarrier	Not mentioned	10 nm	Spherical	(220), (311), (400), (422), (511), and (440)	Spinel [65]
9.	Ag@Fe_3O_4	140 nm	Not mentioned	Spherical	(220), (311), (400), (422), (511), and (440) [66]	Not mentioned
10.	Chitosan-coated iron oxide nanoparticles	Greater than 20 nm	19 nm	Not mentioned	(220), (311), (400), (422), (511), and (440)	Cubic spinel structure [67]

was used for the elemental analysis or chemical characterization of any material. The Fe_3O_4 nanoparticles were synthesized by Hongwei et al. using co-precipitation method and coated with NiS characterized by EDS. It was concluded that a small amount of Ni and S was equally distributed on the surface of synthesized Fe_3O_4 nanoparticles [70].

Lesbayev et al. prepared magnetite nanoparticles by liquid phase chemical condensation method. The elemental percentage composition of O as 25.70% and Fe as 74.30% and no other peaks related with any impurity have been detected in the FESEM-EDS. A sharp peak of Fe was observed at 6.7 keV, and two other peaks around 0.8 and 7.3 keV were found to be observed. A single peak was observed at 0.5 keV for oxygen atom [71]. Cheera et al. synthesized the Fe_3O_4 nanoparticles using extract of Pistum sativum and it was an ecofriendly method. The prepared PS-Fe_3O_4 nanoparticles were characterized by EDS for elemental composition analysis. The deep root observed that the elemental iron present in the Fe_3O_4 nanoparticles. A high intensity peak was observed for Fe at 6.2 keV with other peaks of Fe and there were no other elements observed [48].

2.4 FT-IR Analysis

The energy of most molecular vibrations corresponded to the infrared region of electromagnetic spectrum. The molecular vibrations were detected and measured by either in an infrared spectrum or indirectly Raman spectrum. FT-IR was used to study the surface groups of the assynthesized magnetic nanoparticles, and the achievement of the bonding result was illustrated by the FT-IR spectra. FT-IR was used to identify the organic, polymer and certain inorganic compounds, and the molecular components with its structure efficiency. Peng an et al. prepared the dopamine (DA)-coated Fe_3O_4 nanoparticles by ligand exchange of oleic acid (OA) on Fe_3O_4 nanoparticles and characterized. In FT-IR analysis, the characteristic band due to OA-Fe_3O_4 was observed in the region at 2920 cm^{-1} and at 2851 cm^{-1}. The stretching frequencies such as 1524 cm^{-1} and 1409 cm^{-1} were indicated two carboxylate groups chemisorbed in Fe_3O_4 nanoparticles. DA-Fe_3O_4 showed the absorption band at 1616 cm^{-1} due to –NH stretching, benzene C–C stretching at 1485 cm^{-1}, and phenolic –OH at 1264 cm^{-1}. All the peaks assigned to OA- Fe_3O_4 disappeared in DA-Fe_3O_4 which has been showed the ligand exchange [72].

Fe_3O_4 magnetic nanoparticles (MNP), tannic acid–modified Fe_3O_4 magnetic nanoparticles (TN-MNP), and trypsin-tannic acid-Fe_3O_4 magnetic nanoparticles (TTA-MNP) were prepared by Keziban et al. and characterized by FT-IR studies. The peak at 1706 cm^{-1} confirmed the –C=O group. The characterized band for tannic acid group was confirmed by –O–H or –C–H stretching frequency observed at 2925 cm^{-1} and 2860 cm^{-1}. The broad band was observed at 3600–3100 cm^{-1} due to the phenolic –O–H stretching and methylol group present in tannic acid. The stretching vibration at 1000–1700 cm^{-1} and 3600–3100 cm^{-1} was due to the presence of trypsin enzyme and the presence of phenolic group in TTA-magnetite nanoparticles. The range of 3600–3100 cm^{-1} belonged to the free hydroxyl group present in tannic acid magnetite nanoparticles which has not been participated with the trypsin enzyme [73]. Superparamagnetic magnetite nanoparticles were synthesized by Chengliang et al., and the nanoparticles were characterized by FT-IR analysis where Fe–O bonds stretching band observed at the peak at 557 cm^{-1}. Additionally, the N–H stretching vibration and N–H bending vibration have showed two bands at 3445 cm^{-1} and 1640 cm^{-1} respectively. The peaks at 634 cm^{-1} and 582 cm^{-1} showed the characteristic absorption bands of maghemite (γ-Fe_2O_3), and there were Fe–O frequency deformations in the tetrahedral and the octahedral sites. Magnetite nanoparticles showed an absorption line in the range of about 572–582 cm^{-1} due to the presence of stretching of Fe–O in the tetrahedral sites [74].

Ali et al. prepared the iron oxide nanoparticles coated with carboxyl-functionalized PEG (polyethylene glycol) via dopamine (DPA) linker, and the prepared nanoparticles were characterized by FT-IR. Due to the stretching vibration frequency of Fe–O bonds in Fe_3O_4, absorption peak was observed at 567 cm^{-1}. After the process of carboxylation of PEG, COOH group has replaced all the OH groups present in the polymeric chain. Then, the polymer was precipitated using hexane and was dried in an oven to evaluate the PEG diacid. The peak value of 1725 cm^{-1} was related with acidic C=O, indicating the carboxylation of PEG has been done effectively. The IR spectrum of the coated Fe_3O_4 nanoparticles has the peak value of 1560 cm^{-1} significant to the stretching vibration of acidic C=O. These results confirmed the acidic group present on the coated nanoparticles. In the IR spectrum of PEG diacid, the broadening was observed due to the presence of dopamine aromatic ring. Additionally, the C–O–C bond and asymmetric stretching of CH bond showed the absorption peaks at 1105 and 2925 cm^{-1} respectively. Also, the bending vibrations of CH_2 group have been observed at a band of 1427 cm^{-1}. The FT-IR spectrum confirmed the carboxylated polyethylene glycol (PEG-COOH) was successfully grafted onto the Fe_3O_4 nanoparticles surface [75]. Amine-functionalized Fe_3O_4@C nanoparticles were synthesized by solvothermal process, and the stretching vibration of the primary amine ($–NH_2$) group was observed at 3410 cm^{-1} with an intense and broad absorption band of Fe_3O_4@C nanoparticles. The C–N stretching vibration band was at 1365 cm^{-1} and the C–O band observed was at 1455 and 1610 cm^{-1} for symmetric and anti-symmetric stretching vibrations. The $–CONH_2$ and $C–NH_2$ groups were present in large amount shown by the results and were covalently bonded to the carbon framework in the Fe_3O_4@C nanoparticles. The magnetic nanoparticles were observed and showed the characteristic absorption peak at round 580 cm^{-1} [76].

2.5 Raman Spectra of Fe_3O_4 Nanoparticles

Raman spectrum has been used as a supportive tool to differentiate the crystal phases and to identify the molecular vibrations of the Fe_3O_4 nanoparticles. Cheera et al. synthesized the Fe_3O_4 nanoparticles using extract of Pistum sativum, and it was a poor scatterrer of Raman spectra where the samples of iron oxide nanoparticles were kept under low laser powers to undergo phase transformation. The synthesized PS-Fe_3O_4 nanoparticles have showed the spectrum at 668 cm^{-1} for A_{1g}, 538 cm^{-1} for T_{2a}, 306 cm^{-1} for E_g, and 139 cm^{-1} for T_{2g} for the FCC structure of PS-Fe_3O_4 nanoparticles [48]. Prasad et al. prepared the Fe_3O_4 nanoparticles by green synthesis using Ridge gourd as a starting material, and it showed a peak at 670 cm^{-1} for A_{1g} is considered as a large peak, and 538 cm^{-1} for T_{2a}, 303 cm^{-1} for E_g, and 138 cm^{-1} for T_2 were the peaks observed for FCC structure of RG-Fe magnetite nanoparticles [49].

2.6 SEM Analysis

SEM is one of the most widely used techniques used for the characterization of nanomaterials, nanostructures, and the resolution of SEM approaches in a few nanometers. SEM is used to confirm the crystal shape, surface morphology, dispersed and agglomerated nanoparticles, surface functionalizations, and absolute particle size. It also provides the chemical composition information near the surface. Yong et al. synthesized the magnetic Fe_3O_4 nanoparticles via co-precipitation method, and SEM analysis showed the Fe_3O_4 nanoparticles have the crystalline nature with rod-like structure, when prepared in the presence of magnetic field. Fe_3O_4 nanoparticles were prepared in the absence of magnetic field by co-precipitation method and showed the spherical structure observed by SEM [77]. Aldahir et al. prepared the Fe_3O_4-TMSPT-ATM by magnetite nanoparticles coated with 3- (trimethoxysilyl)-1-propanethiol (TMSPT) and modified with 2-amino-5-mercapto-1, 3, 4-thiadiazole (AMT) as a modifier. SEM analysis determined the particle size for about 114 and 149 nm with homogeneous distribution with the cubic shape of the Fe_3O_4 nanoparticles [78].

The iron oxide nanoparticles were synthesized using co-precipitation method by Keziban et al. The nanoparticles obtained by this method were black in color and magnetic powder in nature. SEM image of iron oxide nanoparticles revealed the heterogeneous morphology without porosity of tannic acid (TA)-MNPs and (tannic acid-trypsin) TTA-MNPs which has the particle size approximately less than 5 μm. The prepared MNPs, TA-MNPs, and TTA-MNPs were having the sizes less than 100 nm, and the SEM images were not obtained obviously in lower size. The alteration of magnetite nanoparticles produced the changes in the particle size [73]. Covalent immobilization of trypsin to modify magnetite nanoparticles by solvothermal method and the morphologies of the Fe_3O_4, Fe_3O_4-TA and Fe_3O_4-TA-TR were characterized. SEM images showed a characteristic low magnification of the Fe_3O_4. It has a cauliflower-like magnetite with agglomerate structures with the particle size approximately less than 500 nm due to the magnetic interaction between the particles. After the TA modification, the size of the agglomerate nanoparticles was found to be decreased owing to the fact that TA was coated on nanoparticles by reducing the magnetic interaction that inhibited the agglomeration. Also, trypsin was binded because enzyme immobilization made the Fe_3O_4-TA as a slightly bigger material [79].

Fe_3O_4 nanoparticles were prepared by co-precipitation method. While using the ultrasound waves, the nanoparticles were functionalized by three types of PEG, and the morphology of these nanoparticles was characterized by SEM. SEM images of Fe_3O_4 nanoparticles showed the uniform size of Fe_3O_4@Cs-sPEG and Fe_3O_4@Cs-PEG_2 nanoparticles and spherical in shape. When it was modified with chitosan, there was spherical morphology with no aggregation found. The nanoparticles were found to be the average diameter around 45 nm suitable size for the drug delivery systems [80]. The fiber composite magnetite nanoparticles were synthesized by liquid phase chemical condensation method. The obtained nanomaterials were found to be porous in structure, and the pores were distributed evenly with the diameter of about 5 to 10 μm [71]. Magnetite nanoparticles were prepared by Aldahir et al. using the microwave-solvothermal method. In this method, the magnetite nanoparticles were coated with 3-(trimethoxysilyl)-1-propanethiol (TMSPT) and modified with 2-amino-5-mercapto-1, 3, 4-thiadiazole (AMT). The particle size was around 25 μm with agglomeration connected to a high magnetic saturation. The distribution of particles was identified to be homogeneous with an obvious particle size between 114 and 149 nm. The magnetic nanomaterial showed the cubic shape determined by SEM [78].

2.7 TEM Analysis of Fe_3O_4 Nanoparticles

TEM was used as a tool to determine the grain size, particle morphology, second-phase particles, size distribution, dislocations, density variations, etc. One of the specific advantages of TEM showed the high magnification range of functional materials. Yang et al. reported the pure Fe_3O_4 was aggregated due to its nanosize, and poly (GMA-MATAC) grafted to Fe_3O_4 nanoparticles showed the change in particle size of Fe_3O_4 nanoparticles for about 200–400 nm with well dispersion. This fact has been explained by electrostatic repulsion force and steric hindrance present in the surface of Fe_3O_4 nanoparticles [51]. Citric acid–coated Fe_3O_4 nanoparticles and Fe_3O_4/Au composite nanoparticles were synthesized by Yan et al. using co-precipitation method. The TEM results showed the average particle size of 10 nm for Fe_3O_4/Au composite nanoparticles, and it was darker than citric acid–

modified Fe_3O_4 with the diameter of about 10–30 nm [81]. Jie Zhu et al. synthesized the Fe_3O_4 magnetic nanoparticles, and cyclodextrin (CD) magnetic nanoparticles by electrochemical method showed the spherical or ellipsoidal shape for Fe_3O_4 magnetic nanoparticles and for cyclodextrin (CD) magnetic nanoparticles also. Fe_3O_4 magnetic nanoparticles have been dispersed uniformly, and somehow, it has been agglomerated due to the lack of surfactants. The average size for Fe_3O_4 nanoparticles and cyclodextrin (CD) magnetic nanoparticles was confirmed to be 10 nm and 16 nm respectively [82]. Highly water-dispersible surfactant-stabilized magnetic Fe_3O_4 nanocarriers (SMNCs) were prepared by Bijaideep et al. and were found to be 10 nm with roughly spherical in shape when characterized [65].

Mustafa et al. synthesized the electro-synthesized coated and uncoated magnetite nanoparticles showing the uncoated nanoparticles were agglomerated with the average size identified to be 10 nm. EDTA capped magnetite nanoparticle confirmed to be spherical in shape with the diameter found to be about 15 nm. It showed the less agglomeration due to EDTA capped with core magnetite nanoparticle for better dispersion [60]. Superparamagnetic magnetite nanoparticles were synthesized by Chengliang et al., and the Fe_3O_4 nanoparticles showed irregular shape with the diameter of about 10 nm [74]. Shete et al. synthesized the CS-OA-Fe_3O_4 nanoparticles by alkaline precipitation and showed the bare Fe_3O_4 nanoparticles were extremely agglomerated with the particle size of about 22.87 nm, while CS-OA-coated nanoparticles were finely dispersed with the particle size of about 16.574 nm. Bare Fe_3O_4 nanoparticles have showed the strong dipole-dipole interaction which led to the high particle size of the magnetite nanoparticles. After coating, non-magnetic layer was formed so that the particle size was decreased for the coated Fe_3O_4 nanoparticles [57]. Ali Ebrahimi Fard et al. synthesized the triethylene-glycol modified Fe_3O_4 nanoparticles by thermal decomposition method. The prepared nanoparticles revealed the spherical morphology with average diameter nanoparticles of 11 ± 3 nm and the particle size distribution exposed a narrow distribution for synthesized nanoparticles [59].

2.8 Mossbauer Spectra of Fe_3O_4 Nanoparticles

Mossbauer technique was helpful to identify the iron state in the functional materials and widely employed to study the fine magnetic particles to find information about the electronic, structural, and magnetic properties of magnetic particles. Fe_3O_4 magnetic nanoparticles were coated with oleic acid (Fe_3O_4-OA-MN), and polyethylene glycol (Fe_3O_4-PEG-MN) was synthesized using co-precipitation method by Runa et al. Mossbauer spectra of Fe_3O_4 nanoparticles revealed in hyperfine splitting, two sextets with doublet peaks of 47 and 43 Tesla for Fe_3O_4 magnetic nanoparticles was observed. For Fe_3O_4-OA-MN, hyperfine splitting has been decreased when compared with Fe_3O_4, and isomeric shift was about 0.31 to 0.45 mm s^{-1}. For Fe_3O_4-OA-MN, the quadrapole splitting confirmed to be zero and the quadrapole splitting was found to be 0.20 mm s^{-1} and the spectra of Fe_3O_4-OA-MN and Fe_3O_4-PEG-MN were comparable [83].

2.9 VSM Analysis of Fe_3O_4 Nanoparticles

The magnetic moment of the Fe_3O_4 nanoparticles with high precision was determined using vibration sample magnetometer. Dopamine (DA)-coated Fe_3O_4 nanoparticles were synthesized by ligand exchange of oleic acid (OA) on Fe_3O_4 nanoparticles. Dopamine was found to have high magnetization of 72.87 emu/g due to lower weight, and the paramagnetic property was detected for both nanoparticles by remanent value. DA-Fe_3O_4 showed the good dispersity confirmed by introducing the external magnetic field [73].

Using the modifiers such as 3-(trimethoxysilyl) propyl methacrylate (MPTMS), 3-(triethoxysilyl) propyl methacrylate (MPTES), and triethoxyvinylsilane (VS), Fe_3O_4 nanoparticles were synthesized by Ceren et al. using co-precipitation method. The magnetic properties of Fe_3O_4 and modified Fe_3O_4-MPTMS were measured by VSM at room temperature. The saturation magnetization values were identified to be 58.87 emu/g and 58.49 emu/g for Fe_3O_4 and modified Fe_3O_4-MPTMS respectively. There was no coercivity present in curve showed the superparamagnetic behavior present in the Fe_3O_4 nanoparticles. The VSM results of Fe_3O_4 nanoparticles showed the surface modification which did not changed the magnetic properties [84].

The magnetic properties of prepared Fe_3O_4 and Fe_3O_4 @ SiO_2@PPh_3@$[CrO_3F]^-$ were measured at room temperature. Fe_3O_4 nanoparticles had the 53.35 emu/g value for saturation magnetization, and Fe_3O_4 @ SiO_2@PPh_3@$[CrO_3F]^-$ was found to have 41.4 emu/g of saturation magnetization with superparamagnetic property [85]. A series of Fe_3O_4 nanoparticles were synthesized using various surfactants by microemulsion method. The VSM results showed the saturation magnetization (M_S) values of nanoparticles were around equal to the vacancy numbers and any increase in vacancy number M_S value has started to decrease which led to the crystal perfection of Fe_3O_4 nanoparticles with the influence of M_S. Defect in any crystal led to the decrease in the M_S value. The presence of coercivity and remanence showed the non-superparamagnetic behavior of reported Fe_3O_4 nanoparticles [50]. Citric acid–coated Fe_3O_4 nanoparticles and Fe_3O_4/Au composite particles were synthesized by Yan et al. using co-precipitation method. The magnetic properties of both the iron nanomaterials were measured by VSM. At 300 K, there was no coercivity or remanence showing the superparamagnetic properties. Citric acid–coated Fe_3O_4 and Fe_3O_4/Au composite nanoparticles showed the saturation magnetization value for about 67 and 30.2 emu/g respectively [81]. Figures 4 and 5 show the

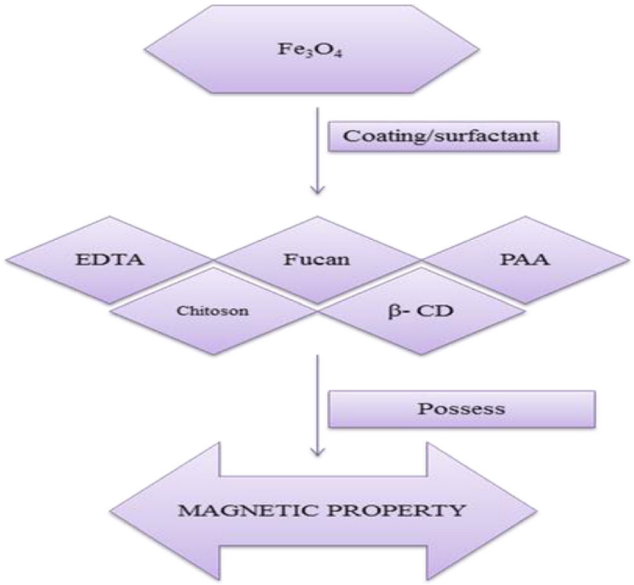

Fig. 4 Iron oxide nanoparticles showing magnetic property

iron oxide nanoparticles and their magnetic property and optical property.

2.10 TGA/DTA Analysis

TGA/DTA analysis was used to determine the thermal stability of fabricated iron nanocomposite. This technique provided the valuable data about the thermal stability of the prepared iron oxide nanoparticles, the bonding strength of the coatings with their surface, and quantitative proof on the structure of the coating agents. The forceful proof of layer-by-layer assembly process was provided by TGA/DTGA results, assigned to the Fe_3O_4-NP, Fe_3O_4-NS (nanoreserviors), and pure NE (nettle extract). At the temperature region from 25 to 150 °C, there was a weight loss due to water adsorption of Fe_3O_4 nanoparticles surface and there was a loss of 2.81%. A weight loss due to the presence of water molecules bounds with Fe_3O_4 nanoparticles surface at the temperature region of about 1.87%. Fe_3O_4 nanoparticles showed the total mass loss was found to be 6.45%. The remaining weight loss at the temperature of 600 °C was due to the conversion of phase transition of Fe_3O_4 to stable FeO. There were three main weight loss steps shown by TGA/DTGA plots of nanoparticles. The temperature ranged from 25 to 150 °C, and a weight loss of about 9.22% was due to the loss of water present in the Nettle structure. In a temperature region of 150–400 °C, there was a weight loss of 36.8% in the decomposition of oxygen-containing groups. The DTGA plot of nanoparticles showed a broad peak consisting of four peaks, and there was intensive and sharp peak at 250 °C and three less intensive peaks at 195, 320, and 370 °C. At temperature higher than 500 °C, there was a weight loss due to the decomposition of aromatic rings. There was a weight loss peak for Fe_3O_4 nanoreserviors observed at 150–300 °C due to the decomposition of NE showing the well loading of inhibitor into the Fe_3O_4-NS. There was another sharp loss peak at 475–525 °C which led to the thermal decomposition of PANI (polyaniline) molecules adsorbed on the Fe_3O_4-NP. The above results validated the precipitation of PANI and NE effectively on the Fe_3O_4-NP surface [86].

The surface property of magnetic nanoparticles was grafted by mono-6-deoxy-6-(p-tolylsulfonyl)-cyclodextrin (6-TsO-CD) and the TGA curves of Fe_3O_4-MNPs, APTES-MNPs (γ-Aminopropyltriethoxysilane), and CDMNPs (cyclodextrins). At 130 °C, there was a weight loss curve of Fe_3O_4-magnetic nanoparticles due to the evaporation of absorbed water and there was a slight weight gain from 130 to 253 °C due to the oxidation of Fe_3O_4 with the total weight loss of Fe_3O_4-MNPs of about 4.2%. The weight loss of about 10.5% at wide temperature range of 230–600 °C due to the role of APTES modified Fe_3O_4-MNPs with the thermal

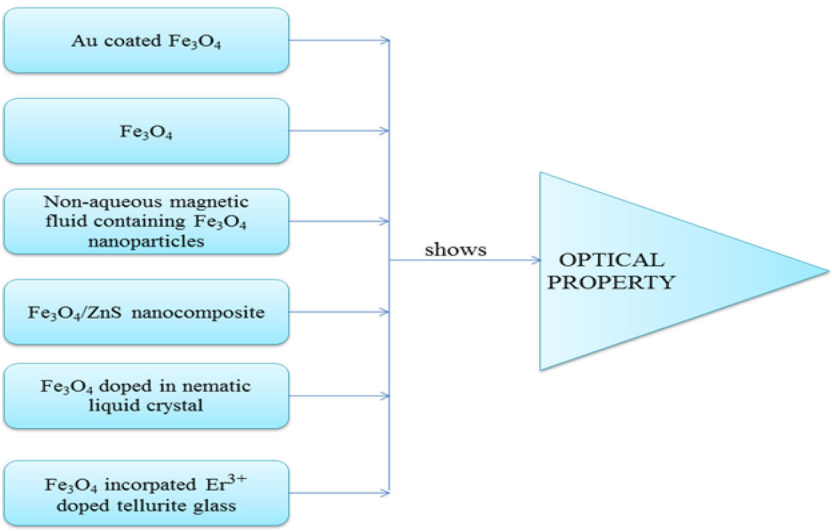

Fig. 5 Flow diagram of iron oxide exhibiting optical property

decomposition of the 3-aminopropyl groups. Upon heating in Ar atmosphere, there were two major weight loss steps. Below 200 °C, there was a loss of residual water adhering to the Fe_3O_4 nanoparticles surface and was adsorbed in the CDs cavities so the weight loss was quite slow. From 200 to 760 °C, a drastic drop loss occurred owing to the thermal decomposition of CDs moieties and other organic structure for the procedure. The better thermal stability of CDs immobilized magnetic nanoparticles because of its cross-linked nature [82].

PEG diacid–grafted Fe_3O_4 nanoparticles were prepared by co-precipitation method and characterized by thermogravimetric analysis. At 100–200 °C, the weight loss of about 5% owing to desorption of water molecules from the surface due to the water withdrawal was hold back. There was a weight loss due to the removal and desorption of immobilized polymeric matrix along with dopamine in the time frame of 200–600 °C. The total weight loss of PEG diacid–grafted Fe_3O_4 nanoparticle was about 22% [75]. Fe_3O_4 nanoparticles modified with gallic acid (MNPs-GA), trypsin immobilization, and protein assay (MNPs-GA-TR) were synthesized and estimated by TG analysis. The TG analysis confirmed the weight loss for magnetic nanoparticles was about 3.57% owing to the loss of water residue. At the temperature range of 40 °C to 900 °C, there was a partial break down of the intermolecular bonds with the successive releasing of volatile fractions led to 5.6% of weight loss occurred for MNPs-GA. In a wide temperature range between 40 and 900 °C, the degradation of gallic acid and trypsin molecules has occurred with the weight loss of about 8.6% [87]. Figure 6 shows the TGA curve of PEG diacid–grafted Fe_3O_4 nanoparticles.

Magnetite Fe_3O_4 nanoparticle was prepared by Teena et al. using co-precipitation method and characterized by TGA. The weight loss of ferric oxide nanoparticles in the temperature test range on the surface was due to the process of physically adsorbed water or chemically attached hydroxyl groups. Other absorbed species like alkaline counter ions coming from the ammonium hydroxide solution used for the co-precipitation method undergone the weight loss beyond 200 °C [88].

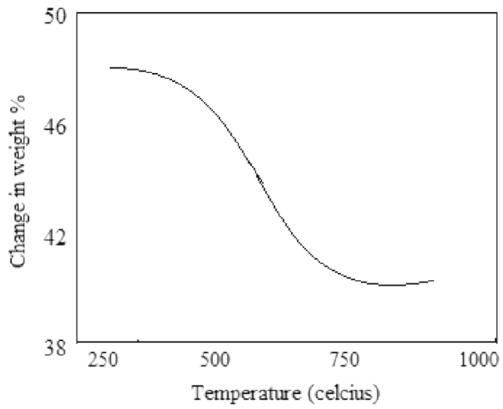

Fig. 6 TGA curve of PEG diacid–grafted Fe_3O_4 nanoparticles

3 Applications

3.1 Removal of Toxic Metal Ions from Aqueous Solutions

Figure 7 shows the application of iron oxide nanoparticles. Domestic and industrial wastewaters discharged into the environment contained various toxic metal ions. These metal ions were not eco-friendly and could not be metabolized by the environment and have the tendency to accumulate in living organisms causing several diseases and disorders. The toxic metals were not destroyed, but they only have been diluted or transformed [89]. Lead and cadmium were the most toxic metals among the various heavy metal ions in the environmental surroundings. The allowable limits of lead and cadmium in wastewater were confirmed to be 0.015 mg/L and 0.01 mg/L respectively [90]. These heavy toxic metal ions have created severe health problems to human beings and animals when the intake was above depicted threshold concentrations. When the consume level has been raised, there was a encephalopathy due to lead, cognitive impairment, behavioral disturbances, kidney damage, anemia, toxicity to the reproductive system, and due to cadmium, nephrotoxic effects, and bone damage–related problems. Hence, there was a need for appropriate method to remove toxic metal ions in the environment [91]. In advanced nanotechnology, magnetic nanomaterials have been combined with magnetic separation, and nanotechnology showed the fine recital in the removal of heavy metal ions from various effluents of the industries [92]. Magnetite (Fe_3O_4) was a ferromagnetic compound with maximum magnetic properties among derivatives of metallic compounds [93]. ID-g-PGMA-MAn composite was

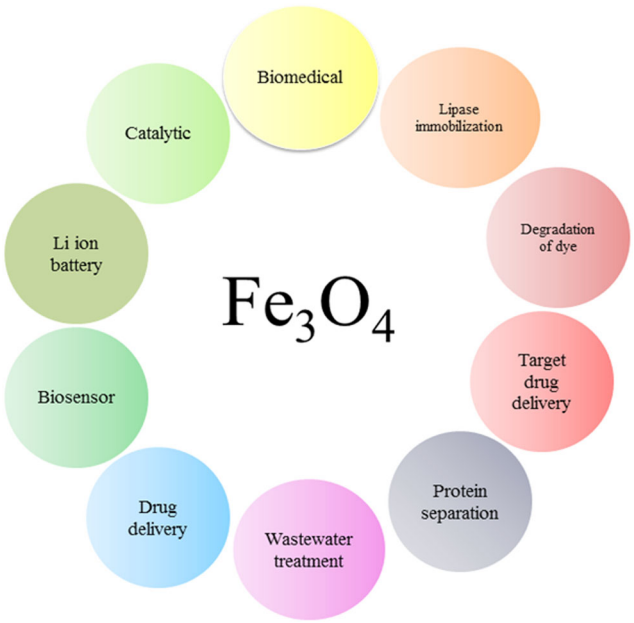

Fig. 7 Application of iron oxide nanoparticle

functionalized and first cross-linked with modified magnetic Fe_3O_4 with amine groups. It was second cross-linked using propylenediamine to enhance the resistance of adsorbent against acid, alkali, and chemicals. The ability of this nanocomposite was studied for removing the Pb (II) and Cd (II) and phenol pollutants from water and wastewater at different conditions. The effect of metal ion concentration on the adsorption process by the magnetic nanocomposite was studied at different concentrations such as 1–40 mg/L. It was reported that the metal ion concentration has increased the removal percentage of metal ions up to 10 mg/L for Pb (II) and Cd (II) ions. When the concentration of metal ions was increased, there was a fall in the removal percentage and could be owed to the saturation of the functional groups in adsorption sites of the adsorbent with the Pb (II) and Cd (II) ions at higher concentrations. There was a need to determine the ions' adsorption process by magnetic adsorbent or not for the Langmuir type adsorption process. From this process, R_L value was calculated and favored the adsorption of heavy metal ions, i.e., Pb (II) and Cd (II). After the removal of toxic metal, a useful metal chelated nanocomposite was obtained. It was a square planar complex which adsorbed the phenoxide ions [94]. Figure 8 illustrates the removal of toxic metal ions and phenol by metal chelated nanocomposite.

3.2 Degradation of Methylene Blue

The most important interest of researchers from chemistry, industry, medicine, physics, biology, and material science towards nanotechnology was to promote the synthesis methods to be easier and cleaner. At present, iron oxide nanoparticles were highly inspiring in research point of view and were considering the dependence of the magnetic properties such as shape, size, composition, surface, and interaction [95]. The green synthesis of iron oxide nanoparticles exhibited the ferromagnetic nature and one of the properties such as catalytic performance of RG-Fe magnetic nanoparticles was studied by UV-vis spectroscopy. The reduction of methylene blue by sodium borohydride in aqueous medium reacted very slowly

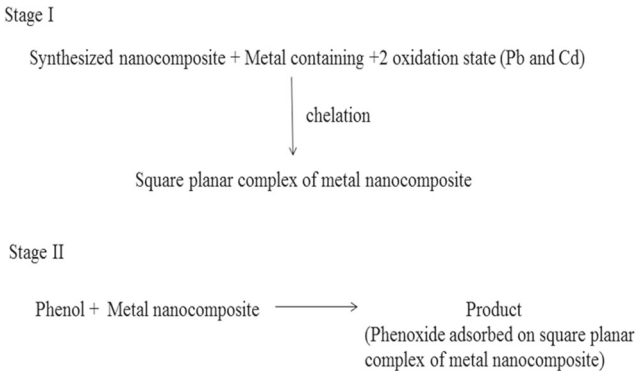

Fig. 8 Removal of toxic metal ions and phenol by metal chelated nanocomposite

without the presence of any catalyst. When the reduction reaction was carried out very rapidly in the presence of RG-FeMNPs as a catalyst using *Ridge gourd*, the UV-visible spectrum was used to fix on the catalytic reduction of the methylene blue molecular structure before and after the removal process of toxic metal ions.

The characteristic absorption band was observed at 650 nm for methylene blue used to study the efficiency of adsorption on RG-FeM nanoparticles. After 30 min, RG-FeM nanoparticles in the presence of $NaBH_4$ have removed the ~96% of the whole methylene blue from the solution better than without the usage of catalyst, and it removed only 13% of methylene blue from the effluent solution. A peak at 650 nm gave the fact that it disappeared within 30 min after adding the RG-FeM nanoparticles as a catalyst. This was due to the presence of double bond cleavage in methylene blue. The observation revealed that comparing with $NaBH_4$ spectrum, the intensity of methylene blue was decreased slowly [49]. Figure 9 reveals the adsorptive property of various types of iron oxides based on its synthesis.

3.3 Polymer-Grafted Magnetic Nanoparticles for Lipase Immobilization

Nowadays, superparamagnetic iron oxide nanoparticles have proved great potential applications in many biological fields like bioseparation, tumor hyperthermia, magnetic resonance imaging (MRI), diagnostic contrast agents, magnetically guided site-specific drug delivery agents, and biomolecules immobilization. The purpose for biomolecules immobilization based on the solid-phase magnetic feature has the ability to achieve a fast and easy separation and to recover the reaction medium in an external magnetic field [13, 96]. The most attractive method in recent days was polymers grafting of magnetic nanoparticles used to analyze the polymer chains that offered flexibility and diversity to control the chemical composition and functional groups on the surface of nanoparticles [97]. Graft polymerization of glycidyl methacrylate (GMA) and methacryloxyethyl trimethyl ammonium chloride (MATAC) onto the surface of modified Fe_3O_4 nanoparticles led to functionalized superparamagnetic particles, and the prepared nanoparticles were used to immobilize the lipase. The surface of vinyl triethoxy silane (VTES) modified-Fe_3O_4 nanoparticles was grafted by GMA and MATAC and induced the large amount of positive electrical charges and reactive epoxy groups on the surface. VTES modified-Fe_3O_4 nanoparticles have immobilized the lipase, and the activity recovery was assayed by hydrolysis of olive oil, and the maximum activity recovery was up to 70.4% [98]. The nanoparticle was added to definite p^H containing the lipase solution. The lipase molecule was first adsorbed and immobilized onto the nanoparticles and the reaction between epoxy groups of the particles and the amino groups. For free lipase and

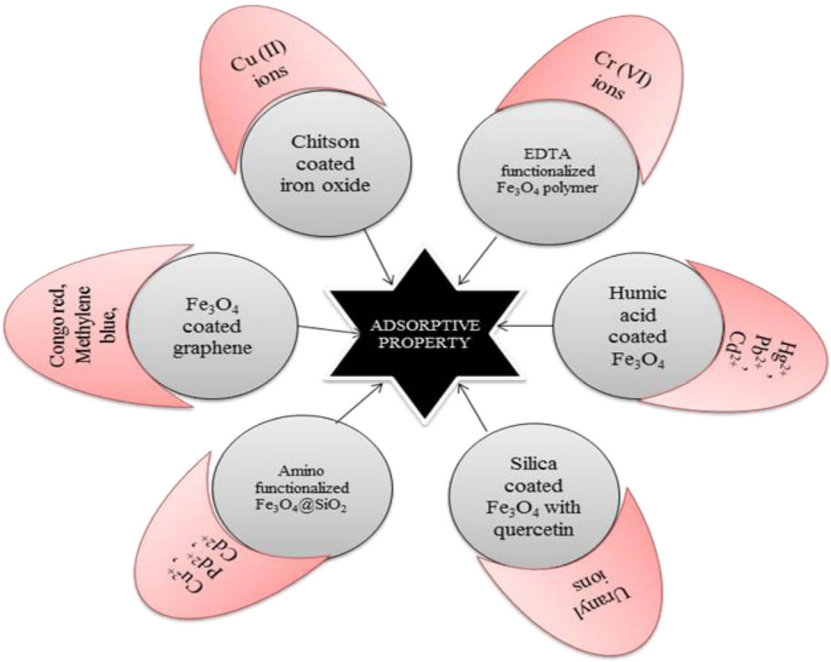

Fig. 9 Adsorptive property of iron oxides

immobilized lipase, thermal stability was determined under some conditions using olive oil. When the temperature was above 40 °C, the immobilized lipase was not inactivated. Also, the temperature was increased, and the activity of free enzyme was decreased. The immobilized lipases at a higher reaction temperature showed the catalytic activities and called as reusability in applications. After a catalysis run, the immobilized lipase was washed with phosphate buffer (0.1 M, p^H 7.0) and reintroduced into a fresh olive oil solution for another hydrolysis at 37 °C. It was experimented that the immobilized lipase has still retained its 70% of activity for after five reuses [51].

3.4 Detection of Zn^{2+} in Soil Samples

For heavy transition metal (HTM) ions and their detections, particular concentration has been focused. Exposure to HTM through different pathways led to the accumulation in human body caused severe illness [99]. In particular, zinc is an essential element and it plays an important role in biological processes (e.g., protein synthesis, neuro transmission, and signal transduction) [100]. The accumulation of zinc in the human body led to the fatal organ failure, copper deficiency, stomach cramps, skin irritations, vomiting, nausea, and anemia [101]. Thus, the detection and removal of Zn^{2+} in contaminated samples were of major interest. Fluorescent sensors were reported as a powerful tool for detecting the metal ions in water and biological samples. The fluorescent sensors for Zn^{2+} have large attention, due to the biological importance of Zn^{2+} ions. Mostly, the sensors were exhibited a poor selectivity for Zn^{2+} ions than the other metal ions. There was difficulty in differentiating Cd^{2+} and Zn^{2+} ions, due to their similar binding properties. Generally, fluorescent molecules were linked to Zn^{2+} chelators such as dipicolylamine (DPA), bipyridine, and cyclic polyamines. [102, 103]. Dopamine-naphthalimide-dipicolylamine was immobilized onto the surface of iron oxide nanoparticle to prepare a hybrid nanomagnet 1- Fe_3O_4 which has the ability to detect Zn^{2+} in soil. The soil was treated with zinc nitrate and incubated for 30 days for the testing of Zn^{2+}. Then, the incubated soil was treated with concentrated nitric acid and extracted. The quantitative analysis of Zn^{2+} was tested by the extract from the contaminated soil and evaluated by fluorescence change of 1-Fe_3O_4. The concentration of Zn^{2+} was found to be 6.3 μM. The value was nearly comparable to the obtained value from ICP-MS (5.9 μM). Thus, 1-Fe_3O_4 showed the potential for the qualitative and quantitate detection of Zn^{2+} present in contaminated soil. Nanomagnet 1-Fe_3O_4 was used for the selective detection and removal of Zn^{2+} from a soil sample and utilized as a capable medium for detecting the Zn^{2+} in various environmental samples [104].

3.5 Removal of Heavy Metal Ions

Magnetite (Fe_3O_4)-mesoporous silica ($mSiO_2$) core-shell nanoparticles were effective and attractive heavy metal ion adsorbents. The results of copper ion adsorption indicated the removal percentage of samples having different pore sizes such as S1-S3 after 50 min was found to be 98.6%, 96.6%, and 89.4%. The removal capacity of S1-S3

was about 84.4, 80.5, and 72.7 mgg^{-1} respectively. All reported studies analyzed the removal of heavy metals using magnetic nanoadsorbents, and the removal capacity was superior to the other materials [105, 106]. Amino-functionalized ferrimagnetic Fe_3O_4-$mSiO_2$ nanoparticles having higher M_s and susceptibility values than superparamagnetic nanoadsorbents have the tendency to capture larger amounts of heavy metal ions in a shorter time. The larger specific surface area and pore size of Fe_3O_4-$mSiO_2$ nanoparticles were found to be major contributions of removal of heavy metal ions [107]. The reusability of the nanoparticles has been established in the view of their valuable use. By measuring the removal efficiency of copper ions after acid treatment, the reusability of Fe_3O_4-$mSiO_2$ nanoparticles was evaluated. Considering sample S1 as a delegate example, the primary removal efficiency was found to be 98.7%, and after acid treatment, the value was decreased to 85%. Finally, it was decreased to 77.2% which confirmed the reusability of Fe_3O_4-$mSiO_2$ nanoparticles. The decrease in efficiency was due to the strong interaction between the amine groups, and the chelating Cu^{2+} ions have not been desorbed enough. The amine groups present in the particles weakly bonded to the SiO_2 surface could be weak to the acid treatment. It showed the removal of cadmium and zinc ions using S1-S3 [108]. The removal efficiency of three metal ions was given in the following order such as $Cu^{2+} > Cd^{2+} > Zn^{2+}$. In general, the −SH group was used to adsorb metal ions such as Hg^{2+}, Ag^{2+}, and Pb^{2+}, through Lewis acid-base interactions, and –COO– groups were used to support the adsorption of ions such as Cu^{2+}, Pb^{2+}, and Cd^{2+} by weak metal-carboxylate interactions. On the other hand, $-NH_2$ groups were well known to bind selectively to Cu^{2+}, Co^{2+}, Ni^{2+}, Pb^{2+}, Cr^{2+}, and Cd^{2+} due to their strong metal complexing capability. Hence, S1 has showed high removal efficiency for Cu^{2+}, Cd^{2+}, and Zn^{2+} [92, 109]. Figure 10 shows the reusability of Fe_3O_4-$mSiO_2$ nanoparticles.

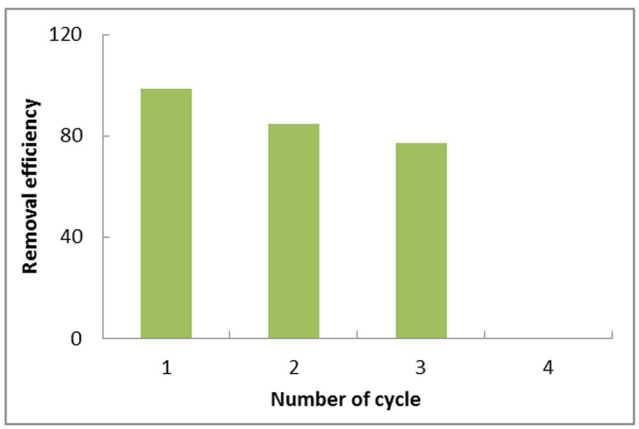

Fig. 10 Reusability of Fe_3O_4-$mSiO_2$ nanoparticles

3.6 Removal of Dyes by Ultrasound Assisted Adsorption

Dyes are the pollutants having the resistant against physical, chemical, and biological treatment processes, and accordingly, their presence in water caused some difficultly and hazardous which root for the researchers to safe treatment of such pollutants [110, 111]. Disulfine blue (DSB) extensively used in wool, silk, carbon paper, cosmetics, and leather activities caused several side effects to eye and skin sensitivity [112]. This inhalation led to the effects of digestion and respiratory tract irritation. Rhodamine 123(R123) was a fluorescent laser dye with high solubility in water which functioned as a tracer in water pollution and aerial pesticide spraying studies and colorant (coloring agent) in drugs, cosmetics, textiles, food stuffs, and inks. When it was swallowed by human and animals, it causes irritation to the skin, eyes, and respiratory tract [113]. Au-Fe_3O_4 nanoparticles-loaded on activated charcoal ($AuFe_3O_4$-NPs-AC) was synthesized and used in water treatment to remove the rhodamine123 (R123) and disulfine blue (DSB) dyes by ultrasound-assisted adsorption. The response surface methodology (RSM) surfaces of DSB and R123 were represented the dye removal percentage versus significant variables. When R123 concentration was raised, DSB removal percentage was decreased automatically. This was due to the increase in ratio of dye molecule to offer surface area for adsorption. It denoted the removal percentage and gradual increased by rising the pH. At low pH, the major event was the protonation of the AC functional groups and most likely, Fe_3O_4 was the adsorbent surfaces that got positive charge. There was a decrease in the DSB removal percentage due to the strong repulsive forces between the cationic dye molecules and adsorbent similar to that of R123. When increase in the initial pH led to deprotonation of the AC, adsorption sites and the OH and COOH corresponded to AC and adsorbed the DSB molecule through electrostatic interaction and/or hydrogen bonding. When there was higher initial dye concentration, the removal percentage of DSB dye was decreased. This was due to the increase in ratio of dye molecule to offer surface area for adsorption. There was a plot between the removal percentage changes versus the adsorbent dosage; dye removal percentage has been increased with increase in adsorbent led to the positive increase of mass. Considerable reduction in removal percentage at minor amount of Au-Fe_3O_4-nanoparticles-AC was attributed to higher ratio of dyes to the vacant sites of the adsorbent. The interaction of pH and R123 concentration with sonication time, R123 removal percentage significantly has the positive relation with sonication time. The rapid shift of dyes to the adsorbent surface admitted the fast equilibrium and confirmed the suitability and efficiency of ultrasound power as powerful tool for wastewater treatment. It has high available surface area and vacant site of adsorbent, enhancing the interface and driving force because of the rapid

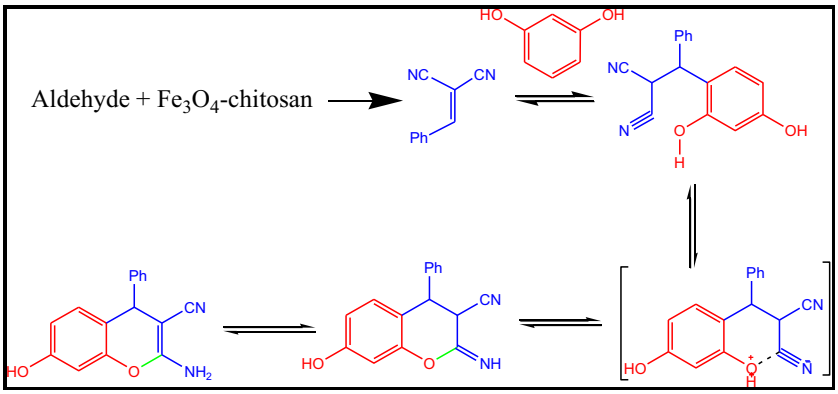

Fig. 11 Mechanism for synthesis of 2-amino-4H-chromenes

initial adsorption rate. Langmuir isotherm explained the formation of monolayer of adsorbate on the outer surface of the Au-Fe_3O_4-NPs-AC. The dyes R123 and DSB on Au-Fe_3O_4-NPs-AC could be well desorbed by 10 mL of acetonitrile solution. The adsorbent was recovered, and the reusability of $AuFe_3O_4$-NPs-AC was tested and examined for four adsorption-desorption cycles. There was no significant loss in the adsorption efficiency observed and the adsorption efficiency of the sixth cycle was reduced by 8.26% compared to that of the first cycle. The desorption capacities were excessive with desorption efficiency of more than 92%. It was concluded that the adsorbent was recycled for both dye adsorptions [114].

3.7 Catalytic Activity

2-amino-4H-chromenes was synthesized by condensation of aldehydes with malononitrile and resorcinol under ultrasound irradiation method. Figure 11 predicts the mechanism for synthesis of 2-amino-4H-chromenes. Using Fe_3O_4-chitosan nanoparticles as the heterogeneous catalysts, the reaction was carried out in a short period of time with the higher yield. The Fe_3O_4 acted as a Lewis acid and the electrophilic character of the aldehyde was increased by the free hydroxyl groups present on the surface of chitosan and could activate the carbonyl group of aldehyde. The nucleophilic property of the malononitrile was activated by the lone pairs of amino group present on the surface of chitosan. The intermediate 2-ethylidene malononitrile may be formed due to Knoevenagel condensation. In this reaction, the intermediate 2-((2,4-dihydroxy phenyl) (phenyl) (methyl)) malononitrile could occur due to Michael addition. An intramolecular cyclization was taken place in the intermediate 2-((2,4-dihydroxy phenyl)(phenyl)(methyl)) malononitrile to give cyclized product and the final product 2-amino-4H-chromenes was obtained. Reusability is the important property for any catalyst. After the reaction completion, ethyl acetate was added and the catalyst was removed by the external magnet. Then, the catalyst Fe_3O_4-chitosan nanoparticles were washed with ethyl acetate. It was dried and used for next cycle reaction without further purification when there was the same substrate. The reusability was checked for the catalyst and it could be reused for four cycles without any loss in its activity [67].

4 Conclusion

In this review, iron oxide nanoparticles have been studied as an exemplary magnetic material. Among the seven phases of iron oxide nanoparticles, Fe_3O_4 exhibited superparamagnetism, and it has inverse cubic spinel structure. Iron oxide nanoparticle was synthesized by various cost-effective methods. The advantages of the synthesis and the properties of iron oxide showed their sustainable and secured use to address the global environmental challenges. This paper reviewed the influence of modifiers on the morphology, structure, size, and optical properties of modified Fe_3O_4 nanoparticles. Fe_3O_4 nanoparticles showed essential applications in supercapacitor electrode materials, magnetic carriers for protein separation, and biomedical applications like targeted drug delivery and catalytic oxidation of alcohols. The catalytic activity of the material was maintained after reuse in several successive cycles of treatment.

References

1. Atkins, P.W., Overton, T.L., Rourke, J.P., Weller, M.T., Armstrong, F. A.: Inorganic Chemistry, 6th Edition. Oxford University Press, Great Britain (2014)
2. Hao, R., Xing, R.J., Xu, Z.C., Hou, Y.L., Gao, S., Sun, S.H.: Synthesis, functionalization, and biomedical applications of multifunctional magnetic nanoparticles. Adv. Mater. **22**, 2729–2742 (2010)
3. Dave, S.R., Gao, X.H.: Monodisperse magnetic nanoparticles for biodetection, imaging, and drug delivery: a versatile and evolving technology. WIREs Nanomed. Nanobiotechnol. **1**, 583–609 (2009)
4. Krishnan, K.M., Pakhomov, A.B., Bao, Y., Blomqvist, P., Chun, Y., Gonzals, M., Giffin, K., Ji, X., Roberts, B.K.: Nanomagnetism and spin electronics: materials, microstructure and novel properties. J. Mater. Sci. **41**, 793–815 (2006)

5. Singh, V., Banerjee, V., Sharma, M.: Dynamics of magnetic nanoparticle suspensions. J. Phys. D. Appl. Phys. **42**, 245006 (2009)
6. Hansen, M.F., Jonsson, P.E., Nordblad, P., Svedlindh, P.: Critical dynamics of an interacting magnetic nanoparticle system. J. Phys. Condens. Matter. **14**, 4901–4914 (2002)
7. Guo, G.Y., Wang, Y.K., Chen, Y.Y.: Ab initio studies of the electronic structure and magnetic properties of bulk and nano-particle $CeCo_2$. J. Magn. Magn. Mater. **272**, e1193–e1194 (2004)
8. Dutta, P., Seehra, M.S., Thota, S., Kumar, J.: A comparative study of the magnetic properties of bulk and nanocrystalline Co_3O_4. J. Phys. Condens. Matter. **20**, 015218 (2008)
9. Cornell, R.M., Schwertmann, U.: The iron oxides: structures, properties, reactions, occurrences and uses. Wiley, Weinheim (2003)
10. Wu, W., Xiao, X.H., Zhang, S.F., Zhou, J.A., Fan, L.X., Ren, F., Jiang, C.Z.: Large-scale and controlled synthesis of iron oxide magnetic short nanotubes: shape evolution, growth mechanism, and magnetic properties. J. Phys. Chem. C. **114**(39), 16092–16103 (2010)
11. Zhang, Z., Boxall, C., Kelsall, G.H.: Photoelectrophoresis of colloidal iron oxides: 1. Hematite (α-Fe_2O_3). Colloids Surf. A Physicochem. Eng. Asp. **73**, 145–163 (1993)
12. Wu, W., He, Q.G., Jiang, C.Z.: Magnetic iron oxide nanoparticles: synthesis and surface functionalization strategies. Nanoscale Res. Lett. **3**, 397–415 (2008)
13. Gupta, A.K., Gupta, M.: Synthesis and surface engineering of iron oxide nanoparticles for biomedical applications. Biomaterials. **26**, 3995–4021 (2005)
14. Kim, Y.S., Kim, Y.H.: Application of ferro-cobalt magnetic fluid for oil sealing. J. Magn. Magn. Mater. **267**, 105–110 (2003)
15. Raj, K., Moskowitz, R.: A review of damping applications of ferrofluids. Trans. Magn. **16**, 358–363 (2002)
16. Schwertmann, U., Cornell, R.M.: The iron oxides: structure, properties, reactions, occurrences and uses, 2nd edn. WILEY-VCH, Weinheim (2003)
17. Schwertmann, U., Cornell, R.M.: Iron oxides in the laboratory. Wiley-VCH, Wienheim (2000)
18. Lu, A.H., Salabas, E.L., Schuth, F.: Magnetic nanoparticles: synthesis, protection, functionalization, and application. Angew. Chem. Int. Ed. Engl. **46**, 1222–1244 (2007)
19. Sun, S.H., Zeng, H.: Size-controlled synthesis of magnetite nanoparticles. J. Am. Chem. Soc. **124**, 8204–8205 (2002)
20. Wang, Z.L.: Transmission electron microscopy of shape-controlled nanocrystals and their assemblies. J. Phys. Chem. B. **104**, 1153–1175 (2000)
21. Xie, J., Xu, C.J., Xu, Z.C., Hou, Y.L., Young, K.L., Wang, S.X., Pourmond, N., Sun, S.H.: Linking hydrophilic macromolecules to monodisperse magnetite (Fe3O4) nanoparticles via trichloro-s-triazine. Chem. Mater. **18**, 5401–5403 (2006)
22. Hou, Y.L., Gao, S., Ohta, T., Kondoh, H.: Linking hydrophilic macromolecules to monodisperse magnetite (Fe_3O_4) nanoparticles via trichloro-*s*-triazine. Eur. J. Inorg. Chem. **2004**, 1169–1173 (2004)
23. Qi, H.P., Chen, Q.W., Wang, M.S., Wen, M.H., Xiong, J.: Study of self-assembly of octahedral magnetite under an external magnetic field. J. Phys. Chem. C. **113**, 17301–17305 (2009)
24. Yang, H.T., Ogawa, T., Hasegawa, D., Takahashi, M.: Synthesis and magnetic properties of monodisperse magnetite nanocubes. J. Appl. Phys. **103**, 07d526–07d529 (2008)
25. Karthikeyan, B., Loganathan, B.: Rapid green synthetic protocol for novel trimetallic nanoparticles. J. Nanopart. **2013**, 1–8 (2013)
26. Zhou, J., Ao, J., Xia, Y., Xiong, H.: Stable photoluminescent $ZnO@Cd(OH)_2$ core–shell nanoparticles synthesized via ultrasonication-assisted sol–gel method. J. Colloid Interface Sci. **393**, 80–86 (2013)
27. Lehui, L., Kelong, A., Yukihiro, O.: Environmentally friendly synthesis of highly monodisperse biocompatible gold nanoparticles with urchin-like shape. Langmuir. **24**, 1058–1063 (2008)
28. Satyavani, K., Gurudeeban, S., Balasubramanian, T.R.: Biomedical potential of silver nanoparticles synthesized from calli cells of Citrullus colocynthis (L.) Schrad. J. Nanobiotechnol. **9**(43), 1–8 (2011)
29. Liang, J., Li, L., Luo, M., Wang, Y.: Fabrication of Fe_3O_4 octahedra by a triethanolamine-assisted hydrothermal process. Cryst. Res. Technol. **46**, 95–98 (2011)
30. Alcala, M.D., Criado, J.M., Real, C.: Synthesis of nanocrystalline magnetite by mechanical alloying of iron and hematite. J. Mater. Sci. **39**, 2365–2370 (2004)
31. Deepika, H., Jacob, L., Rajender, N.N.: A greener synthesis of core (Fe, Cu)-Shell (Au, Pt, Pd, and Ag) nanocrystals using aqueous vitamin C. ACS Sustain. Chem. Eng. **1**, 703–712 (2013)
32. Roy, S., Das, T.K.: Plant mediated green synthesis of silver nanoparticles-a review. Int. J. Plant Biol. Res. **3**, 1044–1055 (2015)
33. O'Handly, R.C.: Modern magnetic materials: principles and applications. Wiley-VCH, Weinheim (2000)
34. Ogielski, A.T., Morgenstern, I.: Critical behavior of three-dimensional Ising spin-glass model. Phys. Rev. Lett. **54**, 928–931 (1985)
35. Saeedi, M.S., Tangestaninejad, S., Moghadam, M., Mirkhani, V., Baltork, I.M., Khosropour, A.R.: Magnetic nanoparticles supported manganese (III) tetrapyridylporphyrin catalyst via covalent interaction: a highly efficient and reusable catalyst for the oxidation of hydrocarbons. Polyhedron. **49**, 158–166 (2013)
36. Zhang, H., Zhu, G.: One-step hydrothermal synthesis of magnetic Fe_3O_4 nanoparticles immobilized on polyamide fabric. Appl. Surf. Sci. **258**, 4952–4959 (2012)
37. Farahani, M.M., Movassagh, J., Taghavi, F., Eghbali, P., Salimi, F.: Magnetite-polyoxometalate hybrid nanomaterials: synthesis and characterization. Chem. Eng. J. **184**, 342–346 (2012)
38. Neel, L.: Magnetic properties of ferrite - ferrimagnetism and antiferromagnetism. Ann. Phys. **3**, 137–198 (1948)
39. Joaquin, G., Gloria, S.: The Verwey transition - a new perspective. J. Phys. Condens. Matter. **16**, R145–R178 (2004)
40. Senn, M.S., Loa, I., Wright, J.P., Attfield, J.P.: Electronic orders in the Verwey structure of magnetite. Phys. Rev. B. **85**, 125119–1251123 (2012)
41. Tilaki, R.M., Iraji zad, A., Mahdavi, S.M.: Stability, size and optical properties of silver nanoparticles prepared by laser ablation in different carrier media. Appl. Phys. A Mater. Sci. Process. **84**, 215–219 (2006)
42. Rao, C.N.R., Muller, A., Cheetham, A.K.: The chemistry of nanomaterials. WILEY-VCH Verlag GmbH & Co. KGaA, Weinheim (2004)
43. Tresintsi, S., Simeonidis, K., Vourlias, G., Stavropoulos, G., Mitrakas, M.: Kilogram-scale synthesis of iron oxy-hydroxides with improved arsenic removal capacity: study of Fe(II) oxidation-precipitation parameters. Water Res. **46**, 5255–5267 (2012)
44. Simeonidis, K., Kaprara, E., Samaras, T., Angelakeris, M., Pliatsikas, N., Vourlias, G., Mitrakas, M., Andritsos, N.: Optimizing magnetic nanoparticles for drinking water technology: the case of Cr (VI). Sci. Total Environ. **535**, 61–68 (2015)
45. Pinakidoua, F., Katsikini, M., Simeonidis, K., Kapraraa, E., Paloura, E.C., Mitrakas, M.: On the passivation mechanism of Fe_3O_4 nanoparticles during Cr (VI) removal from water: a XAFS study. Appl. Surf. Sci. **360**, 1080–1086 (2016)
46. Bhunia, P., Kim, G., Baik, C., Lee, H.: A strategically designed porous iron-iron oxide matrix on graphene for heavy metal adsorption. Chem. Commun. **48**, 9888–9890 (2012)
47. Mi, F., Chen, X., Ma, Y., Yin, S., Yuan, F., Zhang, H.: Facile synthesis of hierarchical core-shell Fe_3O_4@MgAl-LDH@Au as

magnetically recyclable catalysts for catalytic oxidation of alcohols. Chem. Commun. **47**, 12804–12806 (2011)
48. Prasad, C., Yuvaraja, G., Venkateswarlu, P.: Biogenic synthesis of Fe_3O_4 magnetic nanoparticles using Pisum sativum peels extract and its effect on magnetic and methyl orange dye degradation studies. J. Magn. Magn. Mater. **424**, 376–381 (2017)
49. Cheera, P., Karlapudi, S., Sellola, G., Ponneri, V.: A facile green synthesis of spherical Fe_3O_4 magnetic nanoparticles and their effect on degradation of methylene blue in aqueous solution. J. Mol. Liq. **221**, 993–998 (2016)
50. Lua, T., Wanga, J., Yina, J., Wanga, A., Wanga, X., Zhanga, T.: Surfactant effects on the microstructures of Fe_3O_4 nanoparticles synthesized by microemulsion method. Colloids Surf. A Physicochem. Eng. Asp. **436**, 675–683 (2013)
51. Yong, Y., Bai, Y., Li, Y., Lin, L., Cui, Y., Xia, C.: Preparation and application of polymer-grafted magnetic nanoparticles for lipase immobilization. J. Magn. Magn. Mater. **320**, 2350–2355 (2008)
52. Cai, Y., Shen, Y., Xie, A., Li, S., Wang, X.: Green synthesis of soya bean sprouts-mediated superparamagnetic Fe_3O_4 nanoparticles. J. Magn. Magn. Mater. **322**, 2938–2943 (2010)
53. Aslibeiki, B., Kameli, P., Manouchehri, I., Salamati, H.: Strongly interacting superspins in Fe_3O_4 nanoparticles. Curr. Appl. Phys. **12**, 812–816 (2012)
54. Sun, J., Lin, C.: Superparamagnetic POT/ Fe_3O_4 nanoparticle composites with supported Au nanoparticles as recyclable high-performance nanocatalysts. Mater. Today Chem. **5**(43–51), (2017)
55. Silva, V.A.J., Andrade, P.L., Silva, M.P.C., Bustamante, A., De Los Santos Valladares, L., Albino Aguiar, J.: Synthesis and characterization of Fe_3O_4 nanoparticles coated with fucan polysaccharides. J. Magn. Magn. Mater. **343**, 138–143 (2013)
56. Yan, Z., Yuan, J., Zhu, G., Zou, Y., Chen, C., Yang, S., Yao, S.: A new strategy based on cholesterol-functionalized iron oxide magnetic nanoparticles for determination of polycyclic aromatic hydrocarbons by high-performance liquid chromatography with cholesterol column. Anal. Chim. Acta. **780**, 28–35 (2013)
57. Shete, P.B., Patil, R.M., Tiwale, B.M., Pawar, S.H.: Water dispersible oleic acid-coated Fe_3O_4 nanoparticles for biomedical applications. J. Magn. Magn. Mater. **377**, 406–410 (2015)
58. Cevik, E., Senel, M., Baykal, A., Fatih Abasiyanik, M.: Poly (glycidylmethacrylate-co-vinyl ferrocene)-grafted iron oxide nanoparticles as an electron transfer mediator for amperometric phenol detection. Curr. Appl. Phys. **13**, 1611–1619 (2013)
59. Ebrahimi Fard, A., Zarepour, A., Zarrabi, A., Shanei, A., Salehi, H.: Synergistic effect of the combination of triethylene-glycol modified Fe_3O_4 nanoparticles and ultrasound wave on MCF-7 cells. J. Magn. Magn. Mater. **394**, 44–49 (2015)
60. Aghazadeh, M., Karimzadeh, I., Ganjali, M.R.: Ethylenediaminetetraacetic acid capped superparamagnetic iron oxide (Fe_3O_4) nanoparticles: a novel preparation method and characterization. J. Magn. Magn. Mater. **439**, 312–319 (2017)
61. Dhak, P., Kim, M.-K., Lee, J.H., Kim, M., Kim, S.-K.: Linear-chain assemblies of iron oxide nanoparticles. J. Magn. Magn. Mater. **433**, 47–52 (2017)
62. Bajaj, B., Malhotra, B.D., Cho, S.: Preparation and characterization of bio-functionalized iron oxide nanoparticles for biomedical application. Thin Solid Films. **519**, 1219–1223 (2010)
63. Zhu, J., He, J., Du, X., Lu, R., Huang, L., Ge, X.: A facile and flexible process of β-cyclodextrin grafted on Fe_3O_4 magnetic nanoparticles and host–guest inclusion studies. Appl. Surf. Sci. **257**, 9056–9062 (2011)
64. Xu, Y., Zhuang, L., Lin, H., Shen, H., Li, J.W.: Preparation and characterization of polyacrylic acid coated magnetite nanoparticles functionalized with amino acids. Thin Solid Films. **544**, 368–373 (2013)
65. Dutta, B., Shetake, N.G., Barick, B.K., Barick, K.C., Pandey, B.N., Priyadarsini, K.I., Hassan, P.A.: pH sensitive surfactant-stabilized Fe_3O_4 magnetic nanocarriers for dual drug delivery. Colloids Surf. B: Biointerfaces. **162**, 163–171 (2018)
66. Dong, Y., Yang, Z., Sheng, Q., Zheng, J.: Solvothermal synthesis of Ag@Fe_3O_4 nanosphere and its application as hydrazine sensor. Colloids Surf. A Physicochem. Eng. Asp. **538**, 371–377 (2018)
67. Safari, J., Javadian, L.: Ultrasound assisted the green synthesis of 2-amino-4H-chromene derivatives catalyzed by Fe_3O_4-functionalized nanoparticles with chitosan as a novel and reusable magnetic catalyst. Ultrason. Sonochem. **22**, 341–348 (2015)
68. Ma, M., Zhang, Y., Guo, Z., Gu, N.: Facile synthesis of ultrathin magnetic iron oxide nanoplates by Schikorr reaction. Nanoscale Res. Lett. **8**(16), 1–7 (2013)
69. Rahimi, R., Maleki, A., Maleki, S.: Synthesis and characterization of a new magnetic bromochromate hybrid nanomaterial with triethylamine surface modified iron oxide nanoparticles. Chin. Chem. Lett. **25**, 919–922 (2014)
70. Tang, H., Zhang, C., Chang, K., Shangguan, E., Li, B., Chang, Z.: Synthesis of NiS coated Fe_3O_4 nanoparticles as high-performance positive materials for alkaline nickel-iron rechargeable batteries. Int. J. Hydrog. Energy. **42**, 24939–24947 (2017)
71. Lesbayev, A.B., Elouadi, B., Lesbayev, B.T., Manakov, S.M., Smagulova, G.T., Prikhodko, N.G.: Obtaining of magnetic polymeric fibers with additives of magnetite nanoparticle. Procedia Manuf. **12**, 28–32 (2017)
72. An, P., Zuo, F., Yuan Peng, W., Zhang, J.H., Zheng, Z.H., Ding, X.B., Xing Peng, Y.: Fast synthesis of dopamine-coated Fe_3O_4 nanoparticles through ligand-exchange method. Chin. Chem. Lett. **23**, 1099–1102 (2012)
73. Atacan, K., Ozacar, M.: Characterization and immobilization of trypsin on tannic acid modified Fe_3O_4 nanoparticles. Colloids Surf. B: Biointerfaces. **128**, 227–236 (2015)
74. Han, C., Zhu, D., Wu, H., Li, Y., Cheng, L., Hu, K.: TEA controllable preparation of magnetite nanoparticles (Fe_3O_4 NPs) with excellent magnetic properties. J. Magn. Magn. Mater. **408**, 213–216 (2016)
75. Rezayan, A.H., Mousavi, M., Kheirjou, S., Amoabediny, G., Ardestani, M.S., Mohammadnejad, J.: Monodisperse magnetite (Fe_3O_4) nanoparticles modified with water soluble polymers for the diagnosis of breast cancer by MRI method. J. Magn. Magn. Mater. **420**, 210–217 (2016)
76. Lin, J., Wen, Q., Chen, S., Le, X., Zhou, X., Huang, L.: Synthesis of amine-functionalized Fe_3O_4@C nanoparticles for laccase immobilization. Int. J. Biol. Macromol. **96**, 377–383 (2017)
77. Liu, Y., Bai, J., Duan, H., Yin, X.: Static magnetic field-assisted synthesis of Fe_3O_4 nanoparticles and their adsorption of Mn (II) in aqueous solution. Chin. J. Chem. Eng. **25**, 32–36 (2017)
78. Hernandez-Hernandez, A.A., Alvarez-Romero, G.A., Castaneda-Ovando, A., Mendoza-Tolentino, Y., Contreras-Lopez, E., Galan-Vidal, C.A., Paez-Hernandez, M.E.: Optimization of microwave-solvothermal synthesis of Fe_3O_4 nanoparticles. Coating, modification, and characterization. Mater. Chem. Phys. **205**, 113–119 (2018)
79. Atacana, K., Cakiroglu, B., Ozacar, M.: Covalent immobilization of trypsin onto modified magnetite nanoparticles and its application for casein digestion. Int. J. Biol. Macromol. **97**, 148–155 (2017)
80. Khoee, S., Saadatinia, A., Bafkary, R.: Ultrasound-assisted synthesis of pH-responsive nanovector based on PEG/ chitosan coated magnetite nanoparticles for 5-FU delivery. Ultrason. Sonochem. **39**, 144–152 (2017)
81. Xing, Y., Jin, Y.-Y., Si, J.-C., Peng, M.-L., Wang, X.-F., Chen, C., Cui, Y.-L.: Controllable synthesis and characterization of Fe_3O_4/Au composite nanoparticles. J. Magn. Magn. Mater. **380**, 150–156 (2015)

82. Zhu, J., He, J., Du, X., Lu, R., Huang, L., Ge, X.: A facile and flexible process of cyclodextrin grafted on Fe_3O_4 magnetic nanoparticles and host-guest inclusion studies. Appl. Surf. Sci. **257**, 9056–9062 (2011)
83. Ghosh, R., Pradhan, L., Devi, Y.P., Meena, S.S., Tewari, R., Kumar, A., Sharma, S., Gajbhiye, N.S., Vatsa, R.K., Pandey, B.N., Ningthoujam, R.S.: Induction heating studies of Fe_3O_4 magnetic nanoparticles capped with oleic acid and polyethylene glycol for hyperthermia. J. Mater. Chem. **21**, 13388–13398 (2011)
84. Dincer, C.A., Yildiz, N., Aydogan, N., Calimli, A.: A comparative study of Fe_3O_4 nanoparticles modified with different silane compounds. Appl. Surf. Sci. **318**, 297–304 (2014)
85. Rahimi, R., Maleki, A., Maleki, S.: Preparation of magnetic fluorochromate hybrid nanomaterials with triphenylphosphine surface modified iron oxide nanoparticles and their characterization. J. Magn. Magn. Mater. **355**, 300–305 (2014)
86. Izadi, M., Shahrabib, T., Ramezanzadeh, B.: Synthesis and characterization of an advanced layer-by-layer assembled Fe_3O_4/polyaniline nanoreservoir filled with Nettle extract as a green corrosion protective system. J. Ind. Eng. Chem. **57**, 263–274 (2018)
87. Atacan, K., Cakiroglu, B., Ozacar, M.: Improvement of the stability and activity of immobilized trypsin on modified Fe_3O_4 magnetic nanoparticles for hydrolysis of bovine serum albumin and its application in the bovine milk. Food Chem. **212**, 460–468 (2016)
88. Thomas, T., Kanotha, B.P., Nijas, C.M., Joy, P.A., Joseph, J.M., Kuthirummal, N., Thachil, E.T.: Preparation and characterization of flexible ferromagnetic nanocomposites for microwave applications. Mater. Sci. Eng. B. **200**, 40–49 (2015)
89. Fu, F., Wang, Q.: Removal of heavy metal ions from wastewaters: a review. J. Environ. Manag. **92**(3), 407–418 (2011)
90. Musyoka, S.M., Ngila, J.C., Moodley, B., Petrik, L., Kindness, A.: Synthesis, characterization, and adsorption kinetic studies of ethylenediamine modified cellulose for removal of Cd and Pb. Anal. Lett. **44**(11), 1925–1936 (2011)
91. Hutchinson, T.C., Meema, K.M.: In: Hutton, M. (ed.) Lead, mercury, cadmium and arsenic in the environment. Wiley, Hoboken (1987)
92. Ge, F., Li, M.M., Ye, H., Zhao, B.X.: Effective removal of heavy metal ions Cd^{2+} , Zn^{2+} , Pb^{2+} , Cu^{2+} from aqueous solution by polymer-modified magnetic nanoparticles. J. Hazard. Mater. **211**, 366–372 (2012)
93. Zhao, Y.G., Chen, X.H., Pan, S.D., Zhu, H., Shen, H.Y., Jin, M.C.: Self-assembly of a surface bisphenol A-imprinted core–shell nanoring amino-functionalized superparamagnetic polymer. J. Mater. Chem. A. **1**(38), 11648–11658 (2013)
94. Hasanzadeh, R., Moghadam, P.N., Bahri-Laleh, N., Sillanpää, M.: Effective removal of toxic metal ions from aqueous solutions: 2-bifunctional magnetic nanocomposite base on novel reactive PGMA-MAn copolymer@Fe_3O_4nanoparticle. J. Colloid Interface Sci. **490**, 727–746 (2017)
95. Jeong, U., Teng, X., Wang, Y., Yang, H., Xia, Y.: Superparamagnetic colloids: controlled synthesis and niche applications. Adv. Mater. **19**, 33–60 (2007)
96. Krizzova, J., Spanova, A., Rittich, B., Horak, D.: Magnetic hydrophilic methacrylate based polymer microspheres for genomic DNA isolation. J. Chromatogr. A. **1064**, 247–253 (2005)
97. Fan, Q.-L., Neoh, K.-G., Kang, E.-T., Shuter, B., Wang, S.-C.: Solvent-free atom transfer radical polymerization for the preparation of poly(poly(ethyleneglycol) monomethacrylate)-grafted Fe_3O_4 nanoparticles: synthesis, characterization and cellular uptake. Biomaterials. **28**, 5426–5436 (2007)
98. Bradford, M.M.: A rapid and sensitive method for the quantitation of microgram quantities of protein utilizing the principle of protein-dye binding. Anal. Biochem. **72**, 248–254 (1976)
99. Sharma, R.K., Agrawal, M., Marshall, F.: Heavy metal contamination of soil and vegetables in suburban areas of Varanasi, India. Ecotoxicol. Environ. Saf. **66**, 258–266 (2007)
100. Park, S.Y., Yoon, J.H., Hong, C.S., Souane, R., Kim, J.S., Matthews, S.E., Vicens, J.: A pyrenyl-appended triazole-based calix[4] arene as a fluorescent sensor for Cd^{2+} and Zn^{2+}. J. Org. Chem. **73**, 8212–8218 (2008)
101. Plum, L.M., Rink, L., Haase, H.: The essential toxin: impact of zinc on human health. Int. J. Environ. Res. Public Health. **7**, 1342–1365 (2010)
102. Xu, Z., Baek, K.H., Kim, H.N., Cui, J., Qian, X., Spring, D.R., Shin, I., Yoon, J.: Zn^{2+} triggered amide tautomerization produces a highly Zn^{2+} selective cell-permeable, and ratiometric fluorescent sensor. J. Am. Chem. Soc. **132**, 601–610 (2009)
103. Xue, L., Liu, C., Jiang, H.: Highly sensitive and selective fluorescent sensor for distinguishing cadmium from zinc ions in aqueous media. Org. Lett. **11**, 1655–1658 (2009)
104. Kim, K.T., Shin, A., Yoon, J.A., Choi, Y., Lee, M.H., Jung, J.H., Park, J.: Sensors Actuators B. **243**, 1034–1041 (2017)
105. Wang, J., Zheng, S., Shao, Y., Liu, J., Xu, Z., Zhu, D.: Amino-functionalized Fe_3O_4@SiO_2 core–shell magnetic nanomaterial as a novel adsorbent for aqueous heavy metals removal. J. Colloid Interface Sci. **349**, 293–299 (2010)
106. Huang, S.H., Chen, D.H.: Rapid removal of heavy metal cations and anions from aqueous solutions by an amino-functionalized magnetic nano-adsorbent. J. Hazard. Mater. **163**, 174–179 (2009)
107. Jin, S., Park, B.C., Ham, W.S., Pan, L., Young Keun Kim, A.: Physicochemical and engineering aspects. Colloids Surf. A Physicochem. Eng. Asp. **531**(133–140), (2017)
108. Hu, J., Shipley, H.J.: Evaluation of desorption of Pb(II), Cu(II) and Zn(II) from titanium dioxide nanoparticles. Sci. Total Environ. **431**, 209–220 (2012)
109. Ngah, W.S.W., Hanaflah, M.A.K.M.: Removal of heavy metal ions from wastewater by chemically modified plant wastes as adsorbents: a review. Bioresour. Technol. **99**, 3935–3948 (2008)
110. Khattri, S.D., Singh, M.K.: Removal of malachite green from dye wastewater using neem sawdust by adsorption. J. Hazard. Mater. **167**, 1089–1094 (2009)
111. Mittal, A., Kaur, D., Mittal, J.: Batch and bulk removal of a triarylmethane dye, fast green FCF, from wastewater by adsorption over waste materials. J. Hazard. Mater. **163**, 568–577 (2009)
112. Azad, F.N., Ghaedi, M., Dashtian, K., Hajati, S., Pezeshkpour, V.: Ultrasonically assisted hydrothermal synthesis of activated carbon–HKUST-1-MOF hybrid for efficient simultaneous ultrasound-assisted removal of ternary organic dyes and antibacterial investigation: Taguchi optimization. Ultrason. Sonochem. **31**, 383–393 (2016)
113. Baracca, A., Sgarbi, G., Solaini, G., Lenaz, G.: Rhodamine 123 as a probe of mitochondrial membrane potential: evaluation of proton flux through F 0 during ATP synthesis. Biochim. Biophys. Acta. **1606**, 137–146 (2003)
114. Bagheri, S., Aghaei, H., Ghaedi, M., Asfaram, A., Monajemi, M., Bazrafshan, A.A.: Synthesis of nanocomposites of iron oxide/gold (Fe_3O_4/Au) loaded on activated carbon and their application in water treatment by using sonochemistry: optimization study. Ultrason. Sonochem. **41**, 279–287 (2018)